Glassy behaviours in a-thermal systems: the case of granular media

A lecture given in Luxembourg, September 2005

Olivier Dauchot

SPEC, CEA-Saclay, L'Orme des merisiers, 91 191 Gif-sur-Yvette, France

Abstract

Granular media, commonly refered to as a-thermal systems, obey a dissipative dynamics *a priori* very different from an Hamiltonian evolution. However everyday life and recent experiments suggest that a thermodynamical description of granular media might be feasible. Especially in the context of gentle compaction of grains, strong similarities with the behaviour of thermal glassy systems have been underlined. Given that granular media consist in a large number of grains, there is a strong motivation for providing a statistical ground to this hypothetic thermodynamical description. It has been argued by Edwards and collaborators that the dynamics is controlled by the mechanically stable — the so-called blocked — configurations and that all such configurations of a given volume are statistically equivalent This immediately leads to the definition of a configurational entropy and the associated state variable, the compactivity, the formal analogy of a temperature. First attempts to test this flat measure assumption have been conducted. However, clear evidence in real granular media is still lacking. In this lecture, we will first discuss the meaning of thermal vs. a-thermal systems, second review old and new results revealing the strong similarities between granular media close to the jamming transition and super-cooled liquids close to the glass transition, and finally present and discuss Edwards proposal, together with recent experimental results on the volume statistics inside a granular packing.

Contents

1 Introduction **3**

2 Thermal vs. a-thermal systems **4**
2.1 Definitions and general considerations 4
2.2 Illustration in the context of stochastic dynamics 6

3 Glassy behaviour of granular media **9**
3.1 Experimental evidence of the analogy at the macroscopic level 9
3.1.1 Relaxation towards a stationary state 11
3.1.2 Fluctuations of density around the steady state 13
3.1.3 Towards the jammed state 14
3.1.4 Aging and Memory effects 15
3.2 Recent experimental results at the grain scale 17
3.2.1 Fluctuating motion during compaction 17
3.2.2 Cages and diffusion properties without compaction 19
3.2.3 Spatial correlations and dynamical heterogeneities 23
3.3 Partial Conclusion 28

4 Looking for a statistical description **29**
4.1 Edwards' proposal 30
4.2 Experimental test of Edwards' proposal? 32
4.2.1 Volume fluctuations 32
4.2.2 Free volume distributions 33

5 Conclusion and perspectives **37**

Acknowledgements:

The content of these lecture notes owes a lot to my collaborators, without whom none of the present ideas and results would have been developed: G. Marty, F. Da Cruz, F. Lechenault, S. Deboeuf, E. Bertin, G. Biroli. Several papers written with them have inspired the present notes. I want to thank all the members of the "Glassy Work group" in Saclay, in particular, J.P. Bouchaud, E. Vincent, G. Biroli, as well as J. Kurchan, J.M. Lück, C. Godrèche and A. Barrat for many inspiring discussions. I am grateful to the GDR-Midi, which provides an enriching and intellectually challenging context. I want to thank A. Coniglio and his team for having invited me to exchange our views on the topics. Finally let me express my gratitude to M. Henkel and M. Pleimling for giving me the opportunity to give this lecture. Also a special thank to E. Bertin and F. Lechenault for their carefull rereading.

1 Introduction

Granular media composed of large enough grains ($d \geq 250\mu m$) are often refered to as dissipative a-thermal systems. Indeed the energy necessary to move a grain is much larger than $k_B T$, and the interaction between the grains, whether it is friction or inelastic collisions, involves dissipation. For such systems, despite evidences of thermodynamical properties, such as experimentally reproducible relations between macroscopic quantities, a proper statistical approach remains to be constructed. Also, there are many similarities between thermal systems close to the glass transition and granular media close to the so-called jamming transition. These similarities have inspired a lot of recent work towards a statistical description of granular media. However, it is important to note that there are a priori two different issues, one being the description of glassy systems (thermal or not) in the aging regime, the other one being the identification of a precise prescription for the statistical description of a-thermal systems in general. Figure 1 summarises the four corresponding situations which have to be considered.

	Thermal systems	**a-thermal systems**
Stationary dynamics	Gibbs equilibrium	a-thermal stationary states
Aging dynamics	thermal glasses	a-thermal glasses

Figure 1: Equilibrium vs. glassy behaviour of thermal vs. a-thermal systems. Temperature is well defined in the context of equilibrium. Although the present lecture concentrates on the glassy behaviour of granular media (second line of second column), we try in the first section to clarify the difference between thermal and a-thermal systems in the simpler context of stationary dynamics (first line).

In the present lecture, we first try to clarify what is meant — at least here — by a-thermal systems, and present a possible illustration in the context of stochastic dynamics. Then we review experimental results on dense granular media. Some results clearly deal with the glassy behaviour of these systems, others concentrate on the stationary or "super-cooled liquid" regime. In the following, we introduce the prescription proposed by Edwards as a ground for a statistical description of granular media. We discuss the various elements of this proposal, especially focusing on the conditions required to test them experimentally. Finally we present some experimental results on the statistical properties of a dense granular sample.

This lecture is the result of a research under progress. Many concepts remain to be clarified. Despite enormous effort in the recent years, many experimental results are still lacking and those existing may well find new interpretations in a close future due to the progresses on the theoretical side. The reader shall take it as it is : a number of thoughts which we hope will help and motivate him on his way towards the fascinating world of the so-called a-thermal systems.

2 Thermal vs. a-thermal systems

2.1 Definitions and general considerations

We first would like to clarify what we mean by ”dissipative a-thermal system”.

By thermal system one means a system which can couple to the usual thermal environment: the individual components of the system exchange energy with the individual components of the surrounding. The molecules of a gas in a box for instance exchange momentum and thereby kinetic energy with the molecules of the gas surrounding the box. Matter in general is thermal because the microscopic components of matter, the atoms, are of the same scale.

By a-thermal system one means a system whose individual components are of such a large scale compared to the components of the surrounding that the energy received from the thermal environment cannot make them move. One also calls such individual components non-Brownian particles. The thermal environment only contributes to thermalize the matter of which these components are made. Millimetric steel beads for instance won't rearrange by thermal motion, but the steel itself is of course at the room temperature.

Now, a last concept to discuss is dissipation. One needs to consider three scales, the thermodynamic scale, the particles scale and a cutoff scale below which the internal degrees of freedom of the particles are excluded from the description. For instance, in the case of a gas, one may choose to include in the description the electrons and their excitation levels, but not the nucleons. As long as the energy of interaction between the particles is low enough not to excite these sub-cutoff internal degrees of freedom, the dynamics is conservative. Dissipation occurs when there is a flux of energy from the scale of the particles to the scale of the excluded degrees of freedom.

Figure 2 illustrates the above concepts. In the case of usual thermal systems (fig. 2a), the particles inside the system exchange energy with each other and with the particles outside of the system. The dynamics both inside and outside the system is conservative and the internal degrees of freedom are not excited. In the stationary state, the fluxes of energy are described by the usual equilibrium statistical physics, and lead to the equilibration of the well defined usual temperature. In the case of a a-thermal dissipative system surrounded by a usual thermal environment - for instance a granular system in a lab (fig. 2b)- the fluxes of energy are different. The particles inside the system not only exchange energy during their interaction but also excite internal degrees of freedom excluded from the description – such as the phonons. These degrees of freedom, in turn, exchange energy with the thermal environment (fig. 2c). However there is no transfer of energy from the thermal environment to the particles inside the system because of the scale gap. Such a system has to be forced to be maintained in a stationary state different from the rest.

With such images in mind, nothing prevents from imagining the situation where both the system and its surrounding are composed of large scale particles subject to a dissipative dynamics - for instance a small subsystem of a large granular system (fig. 2d). In this case, one recovers a situation similar to that of the usual thermal systems, in the sense that particles inside the system exchange energy with the particles outside the system. However, the dynamics are not conservative anymore. Obtaining a stationary state requires to force both the system and its environment. Whether the fluxes of energy in such a stationary situation could be described by a generalised statistical physics, and thereby a generalised temperature, remains presently an open question of major importance.

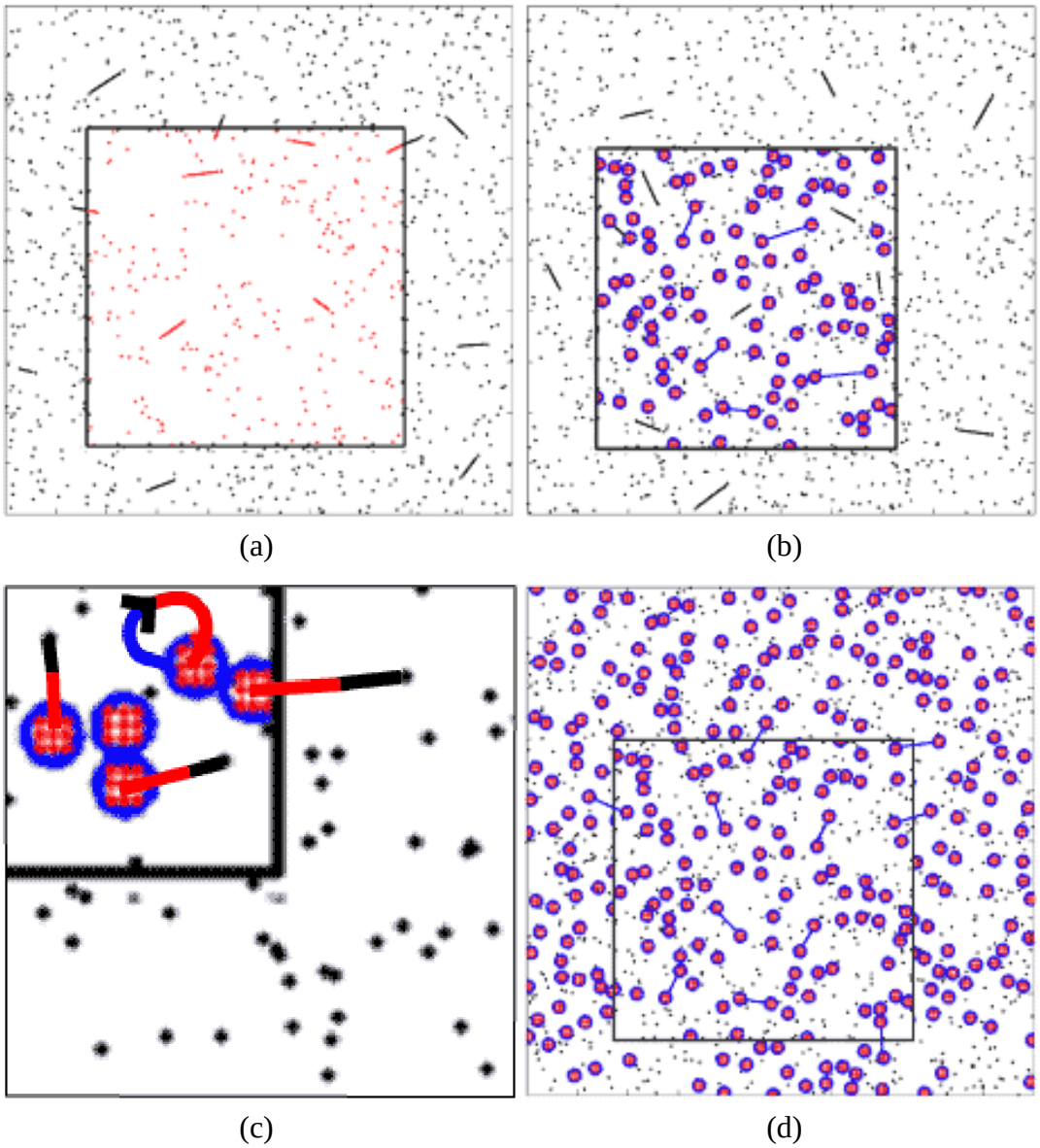

Figure 2: Flux of energies in thermal conservative systems vs. a-thermal dissipative systems. The interactions among the various components are symbolised by straight segments. The dots are particles of gas inside the system in red and outside in dark. The blue circles are grains. The red grids inside the grains symbolise the internal degrees of freedom of the grains. (a): a gas embedded in a gas environment : the particles inside the system exchange energy with each other and with the surrounding particles. (b): a granular media embedded in a gas environment : grains interact with each other; the particle of gas also; the grains do not receive energy from the gas. But, as shown on (c): (zoom of (b)) the grains dissipate – flux of energy towards the internal degrees of freedom, as symbolised by the arrow loop –, which in turn exchange energy with the gas. (d): a subsystem of grains inside a larger system of grains. The gas is ignored in the description. The situation is very similar to that of (a) except for the dissipation which must be taken into account

2.2 Illustration in the context of stochastic dynamics

In the following we will describe a class of systems which may mimic the above situations in the context of a stochastic description – using the master equation formalism.

One crucial goal of a statistical approach for a-thermal dissipative systems would be to give a precise definition of thermodynamical intensive parameters and to predict their relationship with extensive macroscopic variables like energy or volume. Indeed many attempts have been made to define out of equilibrium temperature [15]. In the context of thermal glasses, which we will focus on in the next sections, the notion of effective temperature has been defined recently as the inverse of the slope of the fluctuation-dissipation relation in the aging regime [19]. This definition was inspired by the dynamical results obtained within a class of mean-field spin glass models [18]. A lot of numerical simulations [58, 6, 63, 9, 16] and experiments [37, 7, 39, 22, 2, 64] have been conducted to test the validity of this definition. The situation we want to consider in this section is rather different from that of thermal glasses which are Hamiltonian systems following a non-stationary dynamics with very large relaxation times (first column - second line of figure 1). Here we want to focus on the stationary dynamics of a-thermal particles which follow a non-conservative dynamics (first line - second column of figure 1).

In order to find a stochastic model that describes in the best possible way a given complex Hamiltonian system, without knowing a priori the equilibrium distribution, one should at least preserve the symmetries of the original Hamiltonian system, which are the energy conservation and the time-reversal symmetry $t \to -t$. Energy conservation is easily implemented in the stochastic rules by allowing only transitions between states with the same energy. On the other side, the time-reversal symmetry in the Hamiltonian system can be interpreted in a stochastic language as the equality of two opposite transition rates between the micro-states α and β: $W(\beta|\alpha) = W(\alpha|\beta)$, a property called micro-canonical detailed balance or micro-reversibility. In the context of a dissipative dynamics, the energy is not conserved anymore and one expects the time-reversal symmetry and thereby micro-reversibility to break down. In the most general case, there are little chance to go any further in the description. Following [10, 11] we consider here a subclass of such systems for which we assume that the dynamics still conserves some other quantity — let us call it U.

The stochastic evolution is given by the master equation:

$$\frac{dP_\alpha(t)}{dt} = \sum_\beta W(\alpha|\beta)P_\beta(t) - W(\beta|\alpha)P_\alpha(t) \tag{1}$$

where $P_\alpha(t)$ is the probability of the micros-tate α. In the hamiltonian case, the stationary regime is given by the uniform distribution, $P_\alpha = 1/\Omega(E)$, where $\Omega(E) = \sum_\alpha \delta(E_\alpha - E)$ is the number of states of energy E. When micro-reversibility is broken, the microcanonical stationary distribution is a priori not uniform anymore: $P_\alpha = f_\alpha / Z_\mu(U)$, where f_α is the statistical weight of the configuration α and $Z_\mu(U) = \sum_\alpha f_\alpha \delta(U_\alpha - U)$ can be called a microcanonical partition function. Indeed, the conservation of U was chosen so as to mimic a microcanonical situation. Yet, one sees that the absence of micro-reversibility already yields an important difference, the non uniformity of the stationary distribution.

In order to define a temperature in this context, one can try to follow a procedure similar to that of the equilibrium statistical physics. For an equilibrium system in the microcanonical ensemble, temperature is introduced in the following way. Considering a large system $\mathscr{S}$ with fixed energy, one introduces a partition into two subsystems $\mathscr{S}_1$ and $\mathscr{S}_2$, with energy E_ℓ ($\ell = 1, 2$). These two subsystems can mutually exchange energy; the only constraint is that the total energy $E_{\rm TOT}$ is fixed, and that the energy of interaction is small so that $E_{TOT} = E_1 + E_2$. The key quantity is then the number $\Omega_{\mathscr{S}_1}(E_\ell)$ of accessible states with

energy E_ℓ in the subsystem $\mathscr{S}_\ell$. Assuming that the subsystems do not interact except by exchanging energy, the number of states of the system $\mathscr{S}$ compatible with the partition (E_1, E_2) of the energy is equal to $\Omega_{\mathscr{S}_1}(E_1)\Omega_{\mathscr{S}_2}(E_2)$. Since $E_1 + E_2$ is fixed, the most probable value E_1^* is found from the maximum, with respect to E_1, of $\Omega_{\mathscr{S}_1}(E_1)\Omega_{\mathscr{S}_2}(E_{\rm TOT} - E_1)$. Maximising this product with respect to E_1, one finds the usual result:

$$\left.\frac{\partial \ln \Omega_{\mathscr{S}_1}}{\partial E_1}\right|_{E_1^*} = \left.\frac{\partial \ln \Omega_{\mathscr{S}_2}}{\partial E_2}\right|_{E - E_1^*} \tag{2}$$

Defining the microcanonical temperature T_ℓ of subsystem ℓ by the relation

$$\frac{1}{T_\ell} = \left.\frac{\partial \ln \Omega_{N_\ell}}{\partial E_\ell}\right|_{E_\ell^*} \tag{3}$$

one sees from Eq. (2) that $T_1 = T_2$, i.e. that the temperatures are equal in both subsystems (throughout the lecture, the Boltzmann constant k_B is set to unity). In addition, it can be shown that the common value T does not depend on the partition chosen; as a result, T is said to characterise the full system $\mathscr{S}$.

Very interestingly, this microcanonical definition of temperature can be generalised in a rather straightforward way to the more general case that we consider. Yet, it should be noticed first that microscopic configurations compatible with the given value of the conserved quantity U are not equiprobable, so that $\Omega_{\mathscr{S}}$ is no longer relevant to the problem. But starting again from a partition into two subsystems $\mathscr{S}_\ell = \{\alpha_\ell\} (\ell = 1, 2)$ as above, one can determine the most probable value U_1^* from the maximum of the conditional probability $P(U_1|U_{\rm TOT})$ that subsystem $\mathscr{S}_1$ has $U = U_1$ given that the total conserved quantity is $U_{\rm TOT}$. The conditional distribution $P(U_1|U_{\rm TOT})$ is given by:

$$\begin{aligned} P(U_1|U_{\rm TOT}) &= \sum_{\alpha \in \mathscr{S}} P_\alpha(U_{\rm TOT})\, \delta\left(U_{\alpha_1} - U_1\right) \\ &= \frac{1}{Z_\mu(U_{\rm TOT})} \sum_{\alpha \in \mathscr{S}} f_\alpha\, \delta\left(U_\alpha - U_{\rm TOT}\right)\, \delta\left(U_{\alpha_1} - U_1\right) \\ &= \frac{1}{Z_\mu(U_{\rm TOT})} \sum_{\alpha \in \mathscr{S}} f_\alpha\, \delta\left(U_{\alpha_2} - U_2\right)\, \delta\left(U_{\alpha_1} - U_1\right) \end{aligned} \tag{4}$$

Now assuming — this is a major assumption — that the stationary distribution factorizes (i.e. $f_\alpha(U_1 + U_2) = f_{\alpha_1}(U_1)\, f_{\alpha_2}(U_2)$, one obtains that $P(U_1|U_{\rm TOT})$ may be written in a compact form as:

$$P(U_1|U_{\rm TOT}) = \frac{Z_\mu(U_1)\, Z_\mu(U_{\rm TOT} - U_1)}{Z_\mu(U_{\rm TOT})} \tag{5}$$

This result generalises in a nice way the equilibrium distribution. Indeed at equilibrium $P(E_1|E) = \Omega(E_1)\,\Omega(E - E_1)/\Omega(E)$ and $Z_\mu(U)$ turns precisely into $\Omega(E)$. Finally the most probable value U_1^* satisfies

$$\left.\frac{\partial \ln P(U_1|U_{\rm TOT})}{\partial U_1}\right|_{U_1^*} = 0 \tag{6}$$

which yields

$$\left.\frac{\partial \ln Z_\mu}{\partial U_1}\right|_{U_1^*} = \left.\frac{\partial \ln Z_\mu}{\partial U_2}\right|_{U_{\rm TOT} - U_1^*} \tag{7}$$

So in close analogy with the equilibrium approach, one can define an intensive parameter Y_ℓ for subsystem $\mathscr{S}_\ell$ through

$$\frac{1}{Y_\ell} = \left.\frac{\partial \ln Z_\mu}{\partial U_\ell}\right|_{U_\ell^*} \tag{8}$$

Then Eq. (7) implies that $Y_1 = Y_2$. It can be shown [11] that Y can be computed from the global quantity $Z_\mu(U)$ instead of $Z_\mu(U_1)$ or $Z_\mu(U_2)$, and is thus independent of the partition chosen. This intensive parameter associated to the conservation of the global quantity U characterises the statistical state of the whole system.

Up to now, we have considered only the 'microcanonical' (in a generalised sense) distribution $P_\alpha(U)$. Yet, it would be interesting to introduce also the analogous of the canonical distribution. To do so, one must compute the distribution $P_{\rm can}(\alpha)$ associated to a small (but still macroscopic) subsystem $\mathscr{S}_{\rm can} = \{\alpha\}$ of a large isolated[1] system $\mathscr{S} = \{(\alpha, \alpha')\}$. The configurations corresponding to the reservoir $\{\alpha'\}$ have to be integrated out and one finds under the same assumption of factorizability $f_{\alpha,\alpha'} = f_\alpha f_{\alpha'}$ the following distribution:

$$P_{\rm can}(\alpha) = \sum_{\alpha'} \frac{1}{Z_\mu(U)} f_{(\alpha,\alpha')}\, \delta\left(U_\alpha + U_{\alpha'} - U\right) \tag{9}$$

$$= \frac{1}{Z_\mu(U)} f_\alpha \sum_{\alpha'} f_{\alpha'}\, \delta\left(U_\alpha + U_{\alpha'} - U\right) \tag{10}$$

The above summation is nothing but the microcanonical partition function of the reservoir $Z'_\mu(U - U_\alpha)$, which can be expanded to first order as:

$$\ln Z'_\mu\left(U - U_\alpha\right) = \ln Z'_\mu(U) - \frac{1}{Y} U_\alpha \tag{11}$$

assuming that $U_\alpha \ll U$, which is true as long as $\mathscr{S}_{\rm can}$ is much smaller than $\mathscr{S}$. The derivative of $\ln Z'_\mu(U)$ has been identified with $1/Y$ using Eq. (8). Introducing this last result into Eq. (9), one finally finds

$$P_{\rm can}(\alpha) = \frac{1}{Z_{\rm can}(Y)} f_\alpha \exp\left(-\frac{U_\alpha}{Y}\right) \tag{12}$$

where $Z_{can}(Y) = Z'_\mu(U)/Z_\mu(U)$ –note that U is the conserved quantity of the global system which includes the reservoir and that Y is the associated intensive parameter imposed to the subsystem $\mathscr{S}_{\rm can}$.

At this stage, it is worth making a break and to summarise the above results. Basically, it has been shown that for a stochastic dynamics, which does not conserve energy but conserves another extensive quantity, and which does either not satisfy micro-reversibility :

- one looses the property of uniformity for the probability distribution in the microcanonical ensemble;
- if the microcanonical distribution factorizes, one can still define an intensive parameter associated with the conserved quantity;
- this intensive parameter equilibrates between subsystems;
- one can compute a canonical distribution, which is different from but similar to the Gibbs distribution

The last point calls for a special remark. Because of the factorisation of the distribution in the non-uniform measure and the Gibbs weight, the thermodynamical algebra remains valid. First, one can show that the dynamical entropy defined as

$$S_U(t) = -\sum_\alpha P_\alpha(t) \ln \frac{P_\alpha(t)\delta(U_\alpha - U)}{f_\alpha} \tag{13}$$

[1] Isolated here means that U is conserved inside the large system

is a non-decreasing function of time, which is maximal in the stationary state with the corresponding value $S(U)$ given by:

$$S(U) = -\sum_{\alpha} P_{\alpha}(U) \ln \frac{1}{Z_{\mu}(U)} = \ln Z_{\mu}(U) \tag{14}$$

Second, it is straightforward that

$$\langle U \rangle = -\frac{\partial \ln Z_{\text{can}}}{\partial \gamma} \tag{15}$$

$$\langle U^n \rangle - \langle U \rangle^n = (-1)^n \frac{\partial^n \ln Z_{\text{can}}}{\partial \gamma^n} \quad \text{for} \quad n > 1, \tag{16}$$

where $\gamma \equiv Y^{-1}$. Finally a generalised free energy $F(Y)$ is also naturally introduced through

$$F(Y) = -Y \ln Z_{\text{can}} = \langle U \rangle - Y S \tag{17}$$

To conclude this part we shall say that the above formal analogy, which looks encouraging for further developments, has its drawback : given the very strong similarity at the thermodynamical level with usual thermal equilibrium, it will be experimentally difficult to distinguish between the two statistics. We will come back to this point in section 4.2.

3 Glassy behaviour of granular media

In this part of the lecture we will review a selection of experimental results, which underline the similarity between granular media close to the jamming transition and super-cooled liquids close to the glass transition. It is assumed that the reader is familiar with the glass transition. He might otherwise refer to the other chapters of the present textbook.

3.1 Experimental evidence of the analogy at the macroscopic level

The first set of experimental results concentrates on evidences of the analogy at the macroscopic level. Generically, one considers a three dimensional sample of grains under compaction. We have tried to classify these results according to the following scheme:

- Relaxation towards a stationary state
- Fluctuations and critical slowing down
- Aging and Memory effects

Accordingly we will browse across the results obtained by different groups to illustrate these behaviours. For simplicity we will refer to these experiments by their localisation. Yet, let us first present the various experimental set-up and protocols. Obviously, we can not provide here with all the details of these experiments, which can be found in the original papers.

Figure 3(a) displays the device used in Chicago by Knight et al. [44]. Monodisperse, 2mm diameter glass beads are confined in a 1.88cmm diameter 1m long Pyrex tube mounted on a vibration exciter. The beads are maintained under vacuum. They are prepared in a low density initial stage of packing fraction $\Phi_0 = 0.577$. No convection was observed. The vibration is composed of well separated taps of amplitude a. The acceleration profile of one tap is shown in the inset. $\Gamma = a\omega^2/g$ is the control parameter. The column density was measured with capacitors.

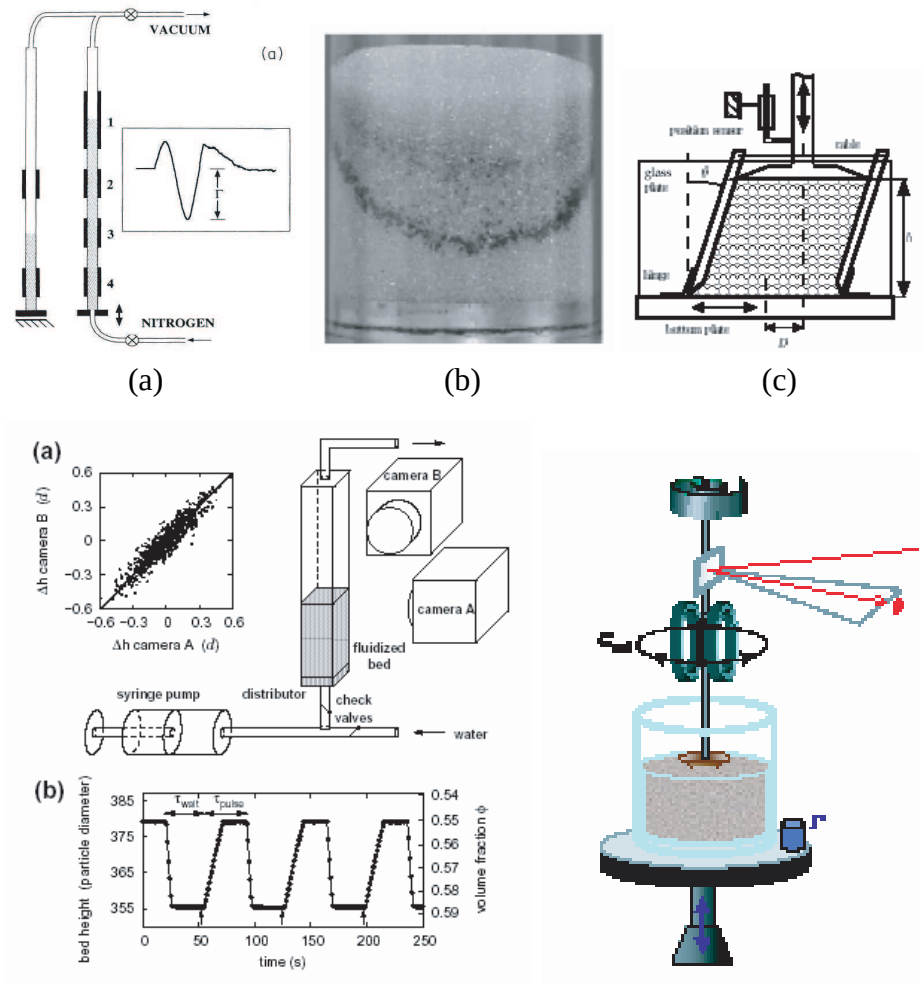

Figure 3: Experimental devices. (a): Compaction under vibration in a large aspect ratio column. Knight et al. [44] (Chicago); (b): Compaction under vibration in a small aspect ratio cell. Philippe et al. [59, 60] (Rennes); (c): Compaction under cyclic shear. Nicolas et al. [56] (Marseille); (d): Compaction in a fluidized bed. Schröter et al. [62] (Austin); (e): Vibration. D'Anna et al. [21, 22] (lausanne).

Figure 3(b) shows a picture of the set-up used in Rennes by Philippe and Bideau [59, 60]. A glass cylinder of diameter 10cm, filled with 1mm diameter glass beads up to 10cm height, is shaken at regular intervals by an electromagnetic exciter delivering independent vertical taps of amplitude a. The experiments start from a reproducible loose packing $\Phi_0 = 0.583$. Boundary effects are restricted but convection is observed. $\Gamma = a\omega^2/g$ is again the control parameter. The average volume fraction in the bulk Φ is estimated by measuring the absorption of a γ-ray beam through the packing.

Figure 3(c) presents a different mode of compaction used in Marseille by Nicolas et al. [56]. A parallelipipedic box (10.5cm high, 7.9cm wide and 10.2cm deep) full of 3mm diameter glass beads is submitted to a horizontal shear through the periodic motion of two parallel walls. The granular packing is confined on the top by a rectangular plate mounted on a vertical rail. The volume fraction during the compaction process is recorded via the vertical position of the top plate. The mean initial volume fraction of the packing is $\Phi_0 =$

0.592. The lateral plates are oscillating quasi-statically between angles $\pm\theta$, θ being the control parameter. The volume fraction is recorded in the vertical position.

Figure 3(d) illustrates the set-up and protocol used in Austin by Schröter et al. [62]. In an original way, the compaction is conducted in a fluidized bed made of a square bore glass tube (24.1mm 24.1mm) filled with about 3.6×10^6 glass beads of $250 \pm 13\mu$m diameter. The beads are fluidized with pulses of temperature-controlled de-ionised water. Flow pulses are generated by a computer-controlled syringe pump so that during a flow pulse the bed expands until its height reaches a stable value. After each flow pulse, the bed settles into a stable time-independent configuration, whose volume fraction is determined by measuring the bed height h with two CCD cameras at a 90° angle.

Finally figure 3(d) displays the apparatus used in Lausanne by D'Anna et al. [21, 22] for studying the jamming transition in weakly perturbed granular media. The granular material, glass beads of diameter $d = 1.1 \pm 0 : 05$mm is contained in a metallic bucket of 150mm height and 94mm diameter, filled to a height of 130mm. The system is subjected to taps, the control parameter being Γ, the peak acceleration of the container, normalised by the acceleration of gravity, g. The granular noise is measured with the help of a torsion oscillator, the rotating probe of which is immersed in the granular material.

Apart from these experiments, we will also discuss the results obtained by Kabla and Debregeas [43] in Paris. In their experiment glass beads of diameter 45μm, contained in a glass cell $(30\text{mm}, 10\text{mm}, 2\text{mm})$, fully saturated with pure water, are very gently vibrated with a piezoelectric actuator on which the cell is rigidly mounted. The mean packing fraction is obtained by measuring the position of the upper surface of the pile with a CCD camera. One tap consists in a train of square wave vibrations. The microscopic dynamics induced by these gentle taps is probed by multi-speckle diffusive wave spectroscopy (MSDWS).

3.1.1 Relaxation towards a stationary state

The very first evidence of a "glassy" behaviour in dense granular media under compaction is the very slow relaxation towards a stationary state with a well defined volume fraction. Figure 4 presents the various compaction curves obtained in the experiments described above. Apart from the experiment in Austin (fig. 4(c)), which is very specific and to which we will come back in more details in section 4.2.1, the number of taps is always counted on a logarithmic scale. For both the experiments in Chicago (fig. 4(a)) and Marseille (fig. 4(b), it is not even clear that a stationary state is reached within the duration of the experiment. In the case of the experiment in Rennes(fig. 4(d), a stationary state is obtained, but for large vibration amplitudes only.

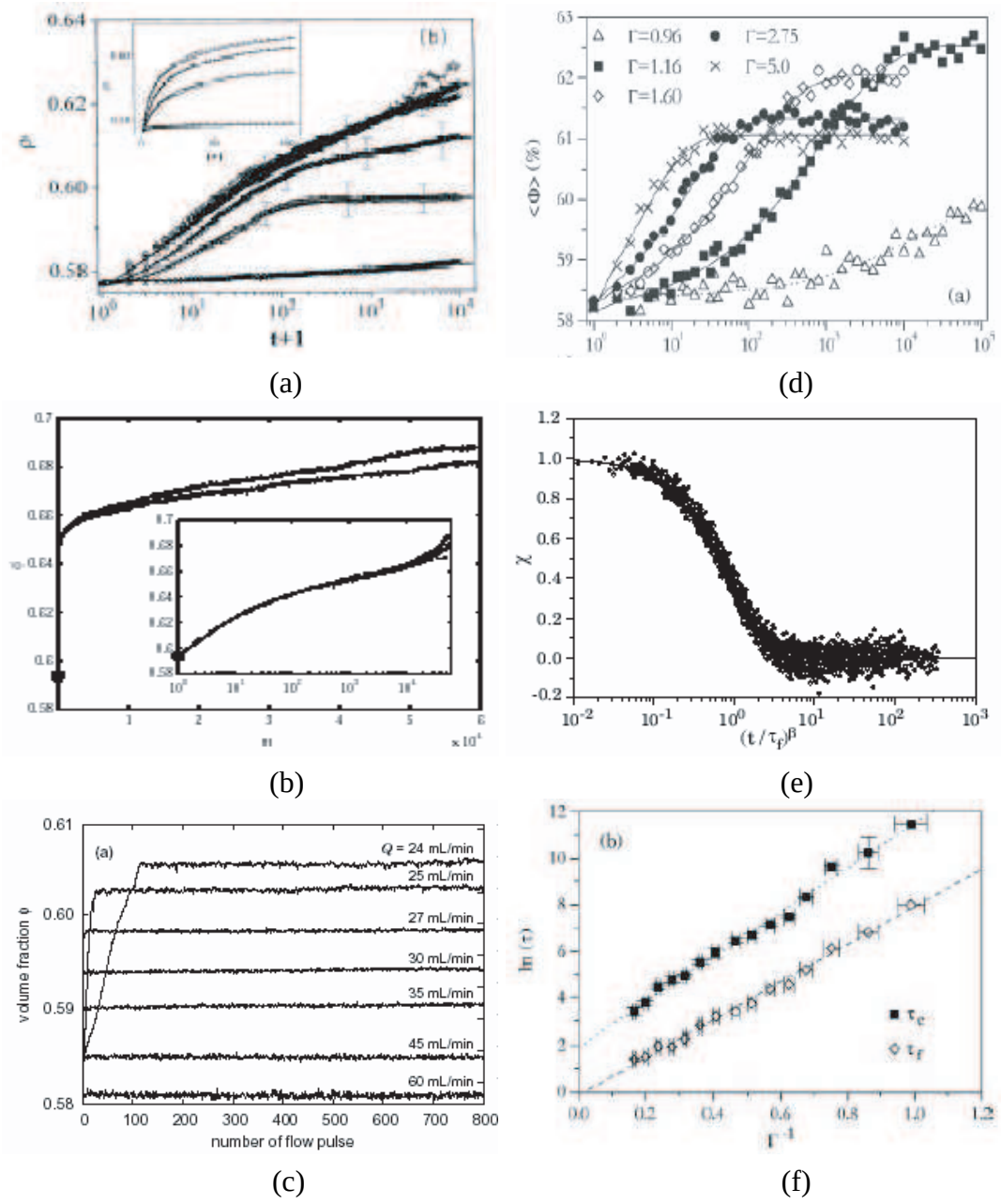

Figure 4: Compaction experiments. (a): Chicago, packing density ρ as a function of the logarithm of the number of tap for various amplitude of vibration ranging from $\Gamma = 1.4$ to 5.4 (inset is the same plot in linear scale); (b): Marseille, compaction curves for $\theta = 5.4°$ for two different runs. Insert: semi-logarithmic scale; (c): Austin, the volume fraction of the sedimented bed for different flow rates Q; (d): Rennes, temporal evolution of the mean volume fraction for different tapping intensities ranging from $\Gamma = 0.96$ to 5.0; (e): Rennes, collapse of the compaction curves obtained with 15 values of Γ between 1.01 and 6.0. $\chi = (\Phi_{ss} - \Phi(t))/(\Phi_{ss} - \Phi(0))$ is plotted as a function of $u = (t/\tau)^{\beta}$. The solid line is the exponential function expected in the case of a stretched exponential law; (f): Rennes, two estimations of the relaxation time τ as functions of the inverse of the tapping intensity Γ.

To be more precise, various fits have been proposed to describe these experimental data. Both Chicago and Marseille experimental data are best fitted by the heuristic expression :

$$\frac{\Phi_\infty - \Phi(t)}{\Phi_\infty - \Phi(0)} = \frac{1}{1 + B\ln\left(1+\frac{t}{\tau}\right)}, \tag{18}$$

whereas Rennes compaction curves are better described by a stretched exponential:

$$\frac{\Phi_\infty - \Phi(t)}{\Phi_\infty - \Phi(0)} = \exp\left[-\left(\frac{t}{\tau}\right)^\beta\right], \tag{19}$$

where Φ_∞, B, τ and $\Phi(0)$ are free parameters depending only on Γ. The latter behaviour, introduced by Kohlrausch [47],Williams and Watts [38], often denoted the KWW law, is commonly observed in the relaxation of thermal glasses, the stretched exponential seemingly indicating the superposition of several relaxation times. Also, in the case of Rennes experiment, the relaxation time dependence is reminiscent of an Arrhenius law $\tau = exp(\Gamma_0/\Gamma)$, for an activated process (fig. 4f). There has been a lot of discussion about the validity of one or the other fit. As a matter of fact, both are plausible in the context of glassy dynamics. The Arrhenius dependence of the relaxation time is reminiscent of strong glasses, whereas one interprets the logarithm dependence as the signature of a fragile glass behaviour. Indeed, as emphasised by Boutreux and de Gennes [13], a Vogel-Fulcher dependence of the relaxation time would lead to a logarithmic relaxation of the density.

3.1.2 Fluctuations of density around the steady state

In statistical mechanics the study of fluctuations can be used to investigate the microscopic states that are accessible to a system maintained at a fixed temperature. In granular media, density fluctuations in the steady state are related to the different volume configurations accessible to the grains subject to an external vibration. We will come back in section 4.1 to the formal analogy proposed by Edwards to relate the role played by vibrations in a-thermal systems, such as granular media, and the role of temperature in thermal systems. For the moment let us come back to some experimental results obtained by Nowak et al. [57] in the Chicago experimental set up.

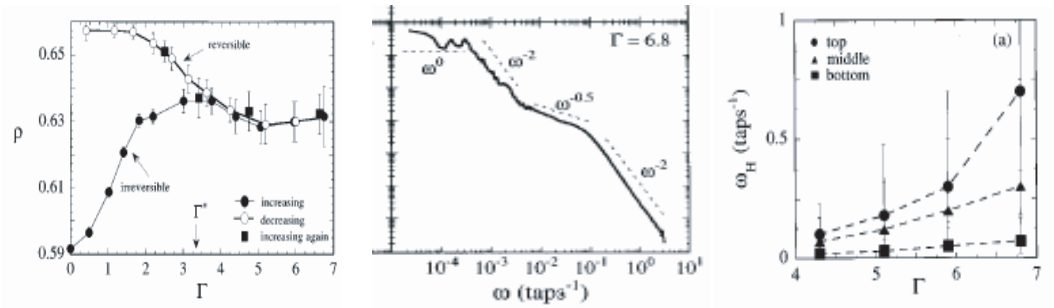

(a) (b) (c)

Figure 5: Density fluctuations around the steady state in Chicago experiment (a): How to reach a reversible steady state branch; The sample is prepared in a low density initial configuration and then the acceleration amplitude is first slowly increased – solid symbols – and then decreased – open symbols. – The upper branch is reversible, see square symbols. (b): Power spectrum of the density fluctuations; (c): Relaxation frequency as a function of the vibration amplitude.

We saw in the above section that for small values of Γ, it is difficult, if not experimentally impossible, to reach a steady-state by merely applying a sufficiently large number of taps of identical intensity. Nowak et al. showed that, in this case, it is possible to reach a steady state by annealing the system 5(a). Experimentally, the value of Γ is slowly raised from 0 to a value beyond $\Gamma^* \simeq 3$, above which subsequent increases as well as decreases in Γ at a sufficiently slow rate $d\Gamma/dt$ lead to reversible, steady-state behaviour. If Γ is rapidly reduced to 0 then the system falls out of the steady state branch. Along the reversible branch, the density is monotonically related to the acceleration. As Γ is increased both the magnitude of the fluctuations around the steady state and the amount of high-frequency noise increase. Figure 5(b) displays the power spectrum of the density fluctuations $S(\omega)$, where the frequency ω is measured in units of inverse taps. Three characteristic regimes emerge: (i) a white noise regime, $S(\omega) \sim \omega^0$ below a low-frequency corner ω_L, (ii) an intermediate-frequency regime with nontrivial power-law behaviour, and (iii) a simple roll-off $S(\omega) \sim \omega^{-2}$ above a high frequency corner, ω_H . As shown on figure 5(c), both ω_L and ω_H increase as Γ is increased. Over the relatively small available range of Γ, the variation of ω_H is consistent with an activated process behaviour: $\omega_H = \omega_0 \exp(-\Gamma_0/\Gamma)$. Approximating to the first order in Γ the bi-univoque relation $\rho(\Gamma)$ characterising the steady state branch, one sees that this mechanically activated law turns into a Vogel-Fuscher dependance in density, compatible with the observed logarithmic relaxation, as emphasised in the previous section. Note that according to this last remark, the distinction between strong and fragile glasses is not really relevant in the case of a transition controlled by density.

3.1.3 Towards the jammed state

The above results were obtained for large enough external solicitations. We will now turn to the behaviour of granular media when the external driving is reduced. Typically one expects a transition close to $\Gamma = 1$ since below this value, the grains are not allowed to lift off from the bottom of the container.

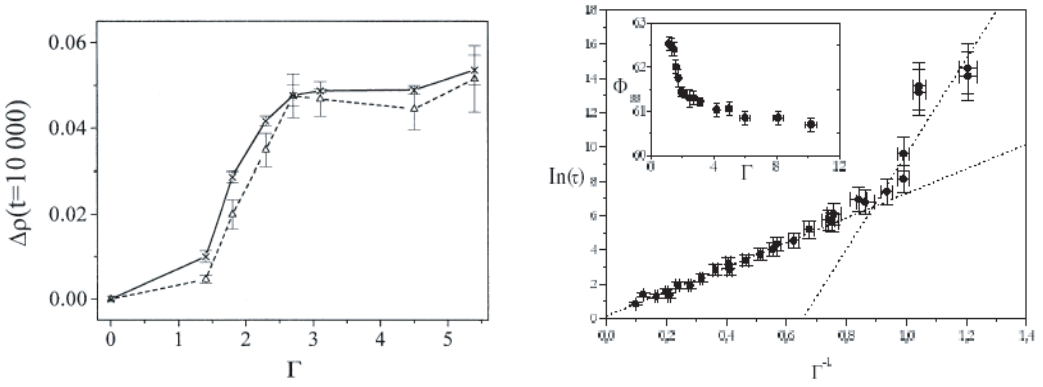

Figure 6: The transition at weak amplitude of vibration (a): 'Asymptotic' (after 10000 taps) density as a function of the vibration amplitude in Chicago experiment (the two curves correspond to two experimental determinations). (b): Arrhenius dependance of the relaxation time as a function of the vibration amplitude in Rennes experiment. Inset: variation of the final volume fraction in the cases where a steady state is actually reached.

This is indeed the case as illustrated on figure 6. In the Chicago experiment (fig. 6a), one sees that the densification after 10000 taps significantly increases for $\Gamma > 1.5$. Note that

this is not a well defined threshold, since it depends on the number of taps, as well as on the details of the experiments. Figure 6(b) shows better evidence of the transition, where one clearly observes a sharp increase of the relaxation times when decreasing Γ below one. The slope variation in the log-lin plot, which indicates a jump in the 'energy barrier' of the mechanically activated process suggested by the Arrhenius laws, finds a natural interpretation in the difference of energy landscape seen by a grain, whether it lifts off or not!

Let us now turn to the Lausanne experiment by D'Anna et al. [21], where a critical slowing down, qualitatively analogous to super-cooling towards the glass transition has been observed. The noise in figure 7(a) exhibits a $1/f^2$ spectrum, characteristic of a diffusive process, even for *Gamma* $\ll 1$. This is already a clear indication that a weakly perturbed granular medium can display a diffusive behaviour well below the fluidization limit.

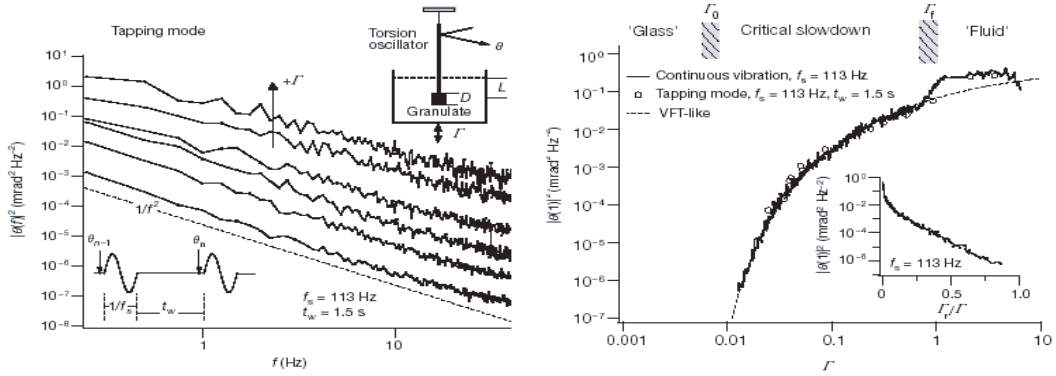

(a) (b)

Figure 7: Towards the jammed state in lausanne experiment (a): Low frequency power spectrum of the torsion oscillator deflection for various intensities of the taps $\Gamma \in [0.025, 3.6]$ (b): Critical slowing down. The power spectrum level at 1 Hz, obtained from continuous vibration measurements. Some points (circles) are obtained from tapping spectra. The dotted line is obtained according to a Vogel-Fuscher fit. Γ_0 is the perturbation intensity where the configuration diffusivity, extrapolates to zero. Γ_f is the fluidization threshold. Inset, the same data as in the main panel in a semilogarithmic plot.

By the Wiener-Khintchine theorem, for a $1/f^2$ noise, the value of the noise at a given frequency is proportional to the diffusion coefficient. Hence, figure 7 displays the characteristic diffusion coefficient as a function of the vibration amplitude for very small amplitude. One observes at $\Gamma_f \simeq 1$ the signature of the vibration-induced fluidization. Second, the diffusion coefficient approaches zero critically, that is, the inverse noise level diverges. This critical approach to zero can be described by a modified Vogel-Fuscher form $A\exp[B(\Gamma-\Gamma_0)^p]$ with $\Gamma_0 = 0.005$ and $p = -0.4$.

All the above results clearly enforce the analogy between the granular behaviour and the physics of glass-forming liquids that super-cool.

3.1.4 Aging and Memory effects

Now that the analogy between thermal glasses and dense granular media has experimental grounds, it is tempting to look for specific behaviours of glasses such as aging and memory effects in granular media close to the jamming transition.

Aging was indeed experimentally observed by Kabla and Debregeas [43] in Paris using multi-speckle diffusive wave spectroscopy (MSDWS) to probe the micron-scale dynamics

of a water saturated granular pile submitted to discrete gentle taps. The pile is first prepared in a reproducible way at low volume fraction, then submitted to high amplitude taps until it reaches a prescribed packing fraction. Only then the dynamics of contacts is probed by submitting the cell to very gentle taps. Figure 8(a) displays the compaction curves during the full procedure. One recognises typical compaction curve during the first stage. In contrast, the low intensity vibrations do not induce significant further evolution of the packing fraction except for initially very loose packs. To quantify the internal dynamics, one measures the intensity correlation of speckle images — produced by the multiple scattering of photons through the sample —, taken between taps, as a function of the number of taps t that separate them. This function generally depends on the total number of small amplitude taps t_w that have been performed. Accordingly one computes the two-times correlation function $g(t_w,t)$:

$$g(t_w,t) = \frac{< I(t_w+t)I(t_w) >_{spkl} - < I(t_w) >^2_{spkl}}{< I(t_w)^2 >_{spkl} - < I(t_w) >^2_{spkl}}, \tag{20}$$

where I is the speckle intensity, $<>_{spkl}$ denotes the average over several speckles.

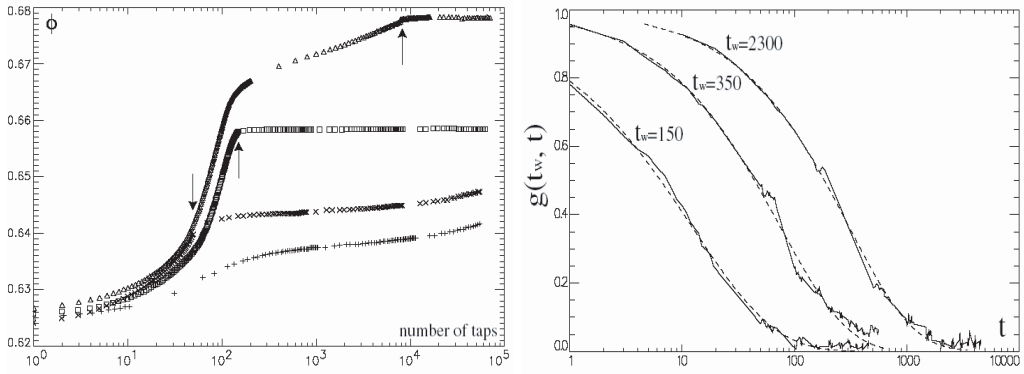

(a) (b)

Figure 8: Aging is a gently vibrated granular media in Paris experiment (a): The packing fraction for four experimental runs. Each run consists of a first step in which high amplitude taps allow rapid compaction of the sample, followed by a sequence of gentle vibrations, during which the internal dynamics is probed. The arrows indicate the change in tapping intensity. (b): Two-time relaxation curves for different waiting time.

Figure 8(b) shows three correlation functions obtained with the same sandpile at different values of t_w. These functions, well fitted by stretched exponentials, clearly demonstrate an increase of the relaxation time with t_w. This dynamical arrest is the signature of the aging behaviour as exhibited in various glassy systems.

As for memory effects, they were observed both in Chicago by Josserand et al. [42] and in Marseille by Nicolas et al. [56]. In the case of Chicago, the granular sample is densified during a set of three experiments up to the same volume fraction Φ_0, but with three different accelerations Γ_0, Γ_1, and Γ_2. After Φ_0 is achieved at time t_0, the system is tapped with the same intensity Γ_0 for all three experiments. As seen in figure 9, the evolution for $t > t_0$ strongly depends on the history, which is the simplest form of memory effect. In the case of Marseille, a periodic shear with inclination angle θ_1 is first imposed to a random packing, and at a given time, the shear amplitude is suddenly changed to another value θ_2 and later switched back to θ_1. As can be seen, increasing the shear angle produces a rapid fall of

volume fraction, followed by a slow and continuous increase. When shear angle is decreased back, a rapid increase of the packing fraction occurs, before recovering the slower one. This is another evidence of memory effect in the packing in the sense that points A and B in figure correspond to packings having the same volume fraction, with different responses to the same shear amplitude.

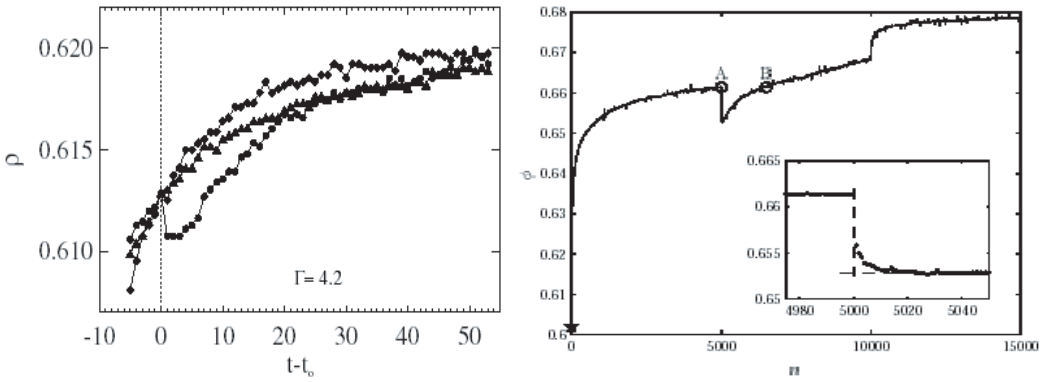

(a) (b)

Figure 9: Memory effect in granular media under compaction. (a): Chicago experiment, time evolution of packing fraction for a system which was compacted to $\rho_0 = 0.613$ at time t_0 using three different accelerations: $\Gamma_1 = 1.8(\bullet), \Gamma_0 = 4.2(\triangle)$, and $\Gamma_2 = 6.3(\diamond)$. After the density ρ_0 was achieved, the system was vibrated at acceleration Γ_0. (b): Marseille experiment, example of angle variation during the compaction process. The insert shows a close-up of the first jump.

Altogether, we have seen in this section that the jamming transition of granular media shares strong similarities — exceedingly slow relaxation, critical slowing down, aging, memory effects — with the glass transition of super-cooled liquids. These similarities are not trivial given the very distinct microscopic processes underlying the dynamics in both systems: in glassy liquids, relaxation occurs by thermally activated rearrangements of the structure. In granular materials, the thermal environment is ineffective and relaxation results from the local yielding of contacts triggered by externally applied vibrations.

3.2 Recent experimental results at the grain scale

In this section, we will report recent experimental results, which deal with the microscopic behaviour of granular materials under cyclic shear. The goal of these experiments is to find a microscopic ground for the analogy evidenced in the previous section. The first experiment was conducted in Marseille by Pouliquen et al. [61] in the device already presented. The second experiment was conducted in Saclay by Marty et al. [54] and Dauchot et al. [23] in a similar device, but significantly different in several aspects. We will first summarise the results obtained in Marseille before describing in more details those, more recent and more complete, obtained in Saclay.

3.2.1 Fluctuating motion during compaction

In Marseilles experiment, the goal was to provide a link between the macroscopic dynamics and the microscopic structure of the packing during compaction by analysing the individual motion of the grain. Accordingly the particles are tracked during compaction using an

index matching method. The first experiments are performed at a constant shear angle. An example of the particle motion is presented in figure 10.1(b), where the plot represents the successive positions of the particles measured after each shear cycle. At first sight particles go down as expected for a macroscopic compaction — see the evolution of the volume fraction in figure 10.1(b)—. On top of this mean vertical displacement, one observes fluctuating motion characterised by ball-like regions as shown in the close-up of figure 10.1(c), revealing a caging process. The random motion of the particles is trapped for a while before escaping and being trapped again in another cage.

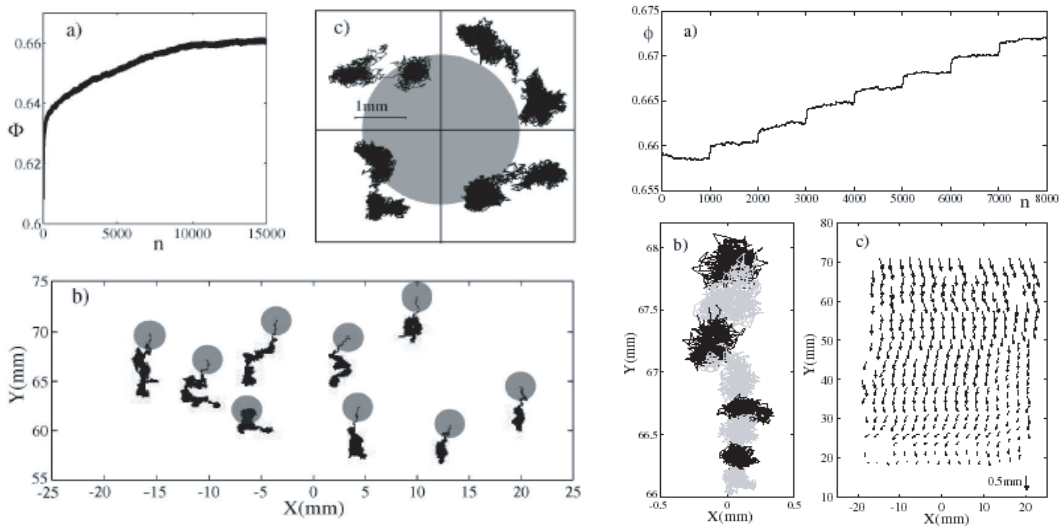

Figure 10: Fluctuating particle motion in Marseille experiment. (1): Compaction for $\theta = 5.4^\circ$; (a) Volume fraction as a function of the number of cycles. (b) Examples of trajectories during 15 000 steps. The disks give the beads size and indicate the initial position of the tracers; (c) Examples of cages (trajectories plotted for time slots between 2500 and 5000 steps). (2): (a) Volume fraction as a function of cycles when θ varies stepwise (see text); (b) Corresponding trajectory of one particle. Changes in colour correspond to changes in θ; (c) Displacement field measured in the cell when θ changes from 10.4° to 1.4°

In order to further investigate the link with compaction , experiments are performed where the shear amplitude is discontinuously decreased. The corresponding volume fraction variation is plotted in figure 10.2(a). As expected from the results presented in the previous section, successive increasing steps in volume fraction are observed. The typical microscopic behaviour of a particle during this experiment is presented in figure 10.2(b). The volume explored by the particle during its random motion successively shrinks when the shear amplitude decreases because the mean particle displacement decreases. However, each time the shear angle changes, the other particles below the test particle experience the same decrease in their exploration volume. The result is a net downward motion observed when the angle changes. The observed volume fraction variation thus results from the change in the volume randomly explored by the particles. This becomes clear in figure 10.2(c) when looking at the displacement of all the particles during a sudden change of shear amplitude. In conclusion a simple scenario can be proposed for the compaction process and its memory effect. The slow dynamics of compaction observed in experiment at a constant amplitude is to be attributed to the changes of cages. These changes are irreversible and push the system towards more and more compact configurations. On the contrary, the rapid change of vol-

ume fraction observed when changing the amplitude is simply related to the change of the cage size, without important structural changes. This explains why this variation of volume is reversible and can be recovered by coming back to the previous amplitude of excitation. The existence of these two processes which affect differently the packing volume fraction explains that memory effects can be observed.

At this stage, it becomes obvious that a detailed statistical study of the particles displacements should bring a lot of information. What are the property of diffusion? The cage changes certainly involve complex cooperative processes. How are the correlations involved in such process? In Marseille experiment, the dynamics is not stationary and particles experience only a few cage changes before being trapped in their final location. Also, it was impossible to follow all particles in their 3D motion.

3.2.2 Cages and diffusion properties without compaction

Answering the above questions in a steady state situation, following all the grains, was the goal of the experimental set up built in Saclay. A prototype of the experimental set-up (figure 11a), allowed Marty and Dauchot to investigate experimentally the diffusion properties of a bi-dimensional bi disperse dry granular material under quasi-static cyclic shear. More specifically, they studied in detail the cage dynamics responsible for the sub-diffusion in the slow relaxation regime, and obtained the values of the relevant time and length scales. In a second version of the set-up (figure 11c), which allows to follow all the grains in a selected area of interest, measurements of multi-point correlation functions are produced. The intermediate scattering function and its self-part, displaying slower than exponential relaxation, suggest dynamic heterogeneity. Further analyses of four point correlation functions reveal that the grain relaxations are strongly correlated and spatially heterogeneous, especially at the time scale of the collective rearrangements. Finally, a dynamical correlation length is extracted from spatio-temporal pattern of mobility. The present section is devoted to the first set of results, the dynamical heterogeneities being described in the next section

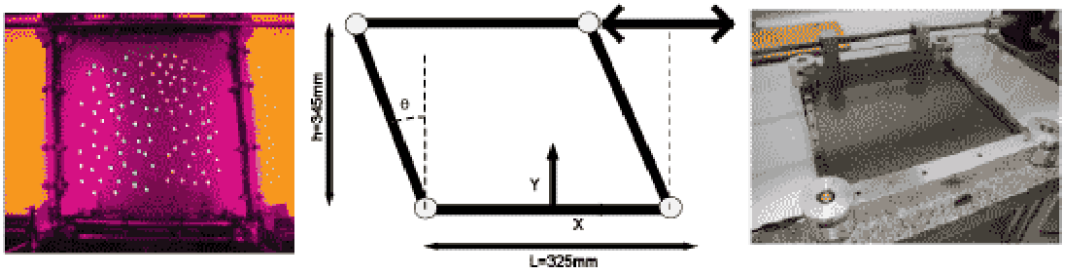

(a) (b) (c)

Figure 11: Experimental set-up; (a) Prototype used for the measurement of the diffusion properties (b) Scheme of the shear cell; (c) Final set-up used for following all grains and measuring the spatio-temporal correlations.

The first experimental setup is as follows: a bi-dimensional, bi-disperse granular material, composed of about 6 000 metallic cylinders of diameter 4 and 5 mm in equal proportions, is sheared quasi-statically in a horizontal deformable parallelogram of constant volume (volume fraction $\Phi \simeq 0.86$). The shear is periodic, with a shear amplitude $\theta_{max} = 10°$. The authors follow a sample of 500 of the grains with a CCD camera which takes a picture of the system each time it comes back to its initial position $(\theta = 0°)$. The unit of time is then one cycle, a whole experiment lasting 10 000 cycles. The unit of length is chosen to be the mean particle diameter d. The system is prepared by removing a fraction of the grains,

shaking the remaining sample, putting back all the grains, and shearing the system during 10 to 20 cycles at high shear amplitude and rate. Figure 12 shows typical trajectories with well identified cages.

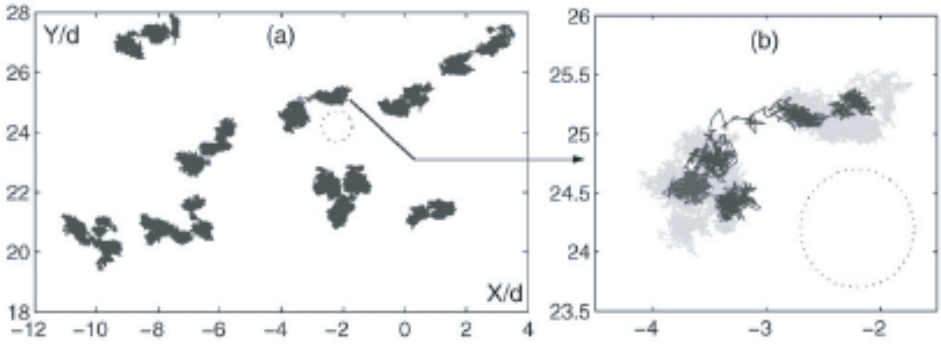

(a) (b)

Figure 12: Evidence of cages. (a) Some tracers trajectories. (b) Gray: a typical trajectory; black: 2000 consecutive steps of the same trajectory. The circle indicates the particle size.

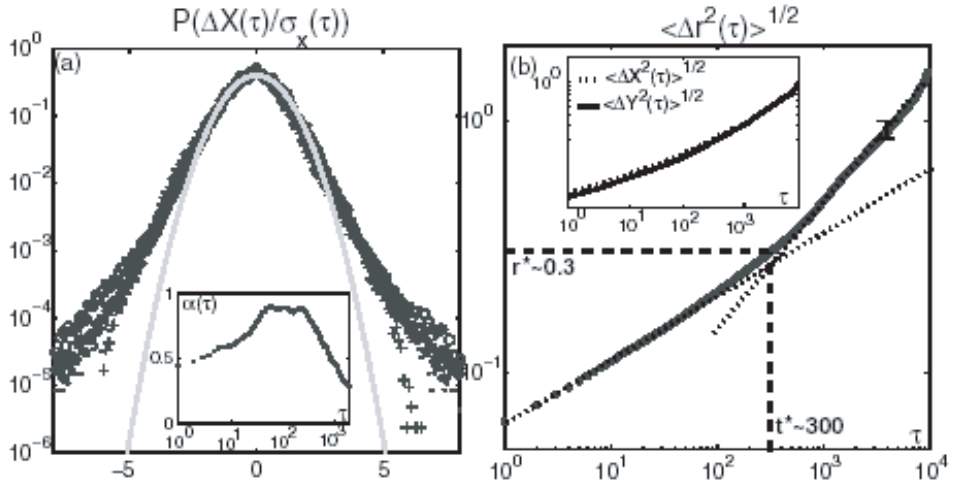

(a) (b)

Figure 13: Diffusion properties (a) pdf of the displacements $\Delta X(\tau)/\sigma_X$ for $\tau = 1(\bullet), 10(\star), 100(\circ), 1000(+)$; the solid line is the Gaussian distribution [inset: non-Gaussian parameter $\alpha(\tau)$]; (b) $\sigma(\tau) = \sqrt{< \Delta r^2(\tau) >}$; dotted lines show the slopes $1/4$ and $1/2$; dashed lines indicate the position of the crossover (r^*, t^*) [inset:$\sigma_X(\tau)$ and $\sigma_Y(\tau)$; no anisotropy is observed].

The probability distribution $P(\Delta X(\tau))$ of the displacements of one particle during a time step τ displayed on figure 13(a) for $\tau = 1, 10, 100, 1000$, exhibit fat tails compared to the Gaussian case, and thereby confirms the intermittent behaviour of the dynamics. The non-Gaussian parameter defined by $\alpha = (< \Delta X^4 > /3 < \Delta X^2 >^2) - 1$ (inset of figure) is indeed different from zero and is maximum, with a plateau, for $\tau \simeq 100$. For larger times, the distribution progressively recovers gaussianity. The root mean square displacement presents two regimes (figure 13b): at short times, the dynamics is sub-diffusive (logarithmic slope $1/4$), while it becomes diffusive (logarithmic slope $1/2$) at long times. These results confirm

and precise the image of particles trapped in cages, where the cage size $r^* = 0.3d$ and the cage lifetime $t^* = 300$ are given by the the crossover between the two regimes.

It is of interest to compare these results with those obtained by Weeks and Weitz [69] in a colloidal suspension of hard spheres, that is a *thermal* system. This system undergoes a glass transition for a packing fraction $\Phi_g = 0.58$. Typical trajectories shown on figure 14(left) and obtained via confocal microscopy for $\Phi = 0.52$ exhibit caged motion, with sudden cage rearrangements. The typical cage size is here also a fraction of the particle diameter. As shown on figure 14(right-a), the motion is diffusive at very short times, then becomes sub-diffusive at intermediate time scales, and finally recovers a diffusive behaviour at large time scales. The sole difference with the granular system is the diffusive motion at very short times, a signature of the thermal activation induced by the solvent of the colloidal suspension. Finally, the non-gaussian parameter (figure 14-right-b) also exhibits a peak which becomes sharper when Φ approaches Φ_g. The type of plateau that has been observed in Saclay typically occurs for $\Phi = 0.52$, that is at a relative distance to transition of 10%.

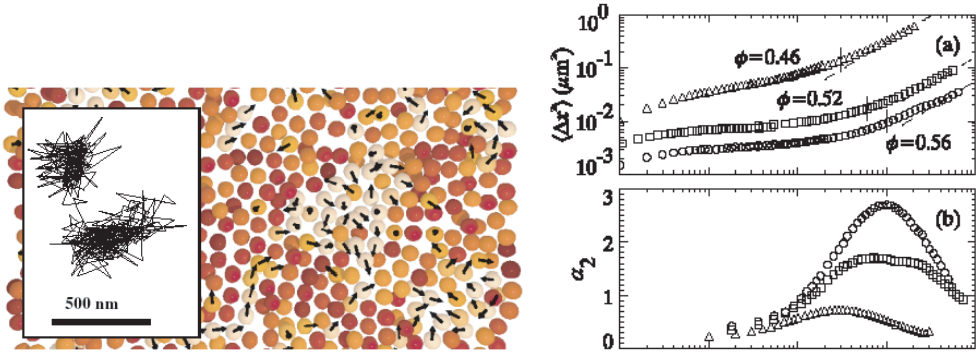

Figure 14: Evidence of cages. Left: one layer of particles through a three-dimensional sample of the colloidal suspension, with arrows indicating the direction of motion for particles with displacements. Lighter colours indicate particles with larger displacements. Inset: 120 min. trajectory of one particle from this sample. Right: (a) Mean square displacements. (b) Non-Gaussian parameter.

Let us now report the kind of analysis that can be conducted to better characterise the dynamics. A very convenient tool introduced by Doliwa and Heuer [26, 27], is the conditional probability $P(x_{12}|r_{01})$ (resp. $P(y_{12}|r_{01})$) of the projection x_{12} (resp. y_{12}) of the displacement during a given time interval τ along (resp. orthogonally to) the direction of the motion during a previous time interval of the same duration τ, conditioned by the length r_{01} of the motion during the previous time interval.

These quantities are displayed on figure 15. A first observation is that the mean value of y_{12} is zero, while the mean value of x_{12} is always negative. More precisely, for a given time interval τ, $< x_{12} >$ decreases linearly with r_{01} for $r_{01} < r^*$, then saturates at a constant negative value. The decrease is stronger for small τ and disappears for $\tau > t^*$. On the contrary, the saturation always occurs at $r_{01} = r^*$, a strong indication that the dynamics is controlled by the cage size. Altogether for displacements smaller than r^*, the larger a step the more anti-correlated is the following step, which reflects a systematic back dragging effect experienced by the particle trapped in its cage. For displacements larger than r^*, a cage rearrangement has occurred, and so the anti-correlation does not increase any more. Yet, the constancy of $< x_{12} >$ at this saturation value reveals some memory of the fact that part of the trajectory was made in a cage. At larger τ these effects become weaker, an indication that cages relax and adapt to the new positions of the enclosed particles. One can even go

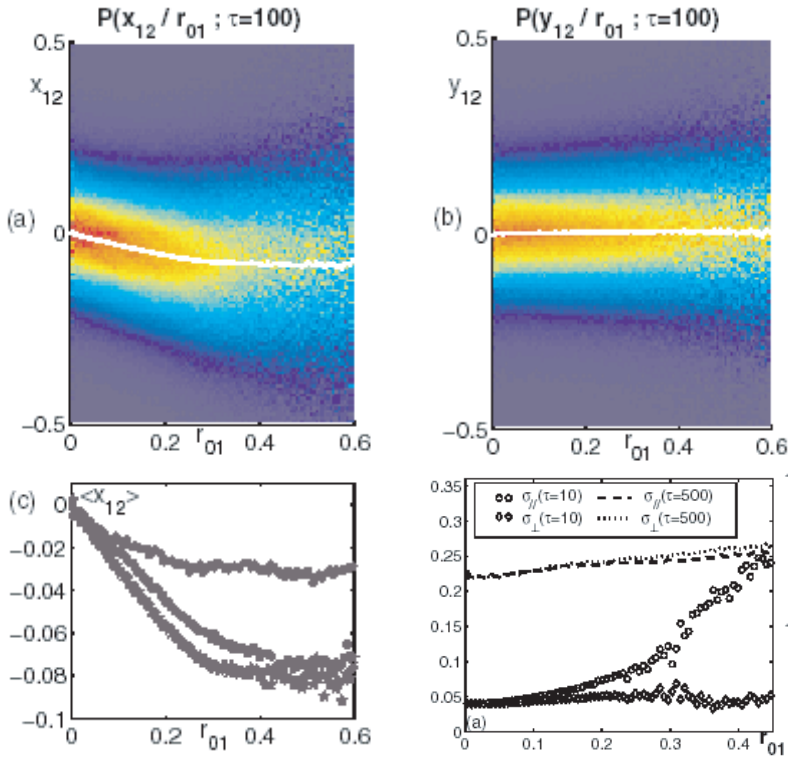

(a) (b)

Figure 15: Temporal correlations. (a) and (b) conditional probabilities (in colour scale) $P(x_{12}|r_{01}$ and $P(y_{12}|r_{01}$; the white traces are the mean values $< x_{12} >$ and $< y_{12} >$; (c) $< x_{12} >$ for different values of τ (from bottom to top: $\tau = 100; 300; 500$) (d) Widths of the distribution of $x_{12}(\sigma_{//})$ and $y_{12}(\sigma_{\perp})$ versus r_{01} for $\tau = 10$ and $\tau = 500$.

further in the interpretation of these distributions by extracting their widths $\sigma_{//}$ and $\sigma_{\perp}$. The increase of $\sigma_{//}$ with r_{01} reveals that large steps are more likely for particles which moved farther during the previous time interval. This is an indication of the existence of a population of fast particles, a typical feature of glass forming systems, as pointed out, for example, in [41, 26, 68]. Second, we see that for short time intervals, the increase of $\sigma_{//}$ is larger than the one of $\sigma_{\perp}$. This reflects some anisotropy in the motion, as observed in the string-like cooperation observed numerically by Donati et al. [28]. Both effects concern movements on short time scales, since they tend to disappear as the time interval τ is increased.

Let us now turn to the investigation of some spatial correlations. We choose to illustrate an other technique introduced by Hurley and Harrowell [41], based on relaxation times. For a particle i, the relaxation time $T_i(r)$ is defined as the time needed by the particle to reach a given distance r for the first time. The distribution of these relaxation times is shown in the inset of figure 16(a), for $r = r^*$.

Defining $T_{i,\ell}(r)$ as the mean relaxation time of the particles contained in a circle of radius ℓ centred on particle i, then the dependance on ℓ of the fluctuations of $T_{i,\ell}(r)$ should provide some information about the typical length L over which cooperative effects take place. A well normalised quantity to compute is $m2_\ell(r) = \left\langle (T_{i,\ell} - T_{i,avg})^2) \right\rangle / \left\langle (T_{i,1} - T_{i,avg})^2) \right\rangle$, where $T_{i,avg}$ is the mean relaxation time averaged over all particles. $m2_\ell(r)$ is plotted versus ℓ for different r on figure 16(a). $m2_\ell(r)$ naturally decreases with ℓ but is not monotonic with r. To quantify this, one can plot L (defined as the integral of $m2$ over ℓ) versus r and obtain

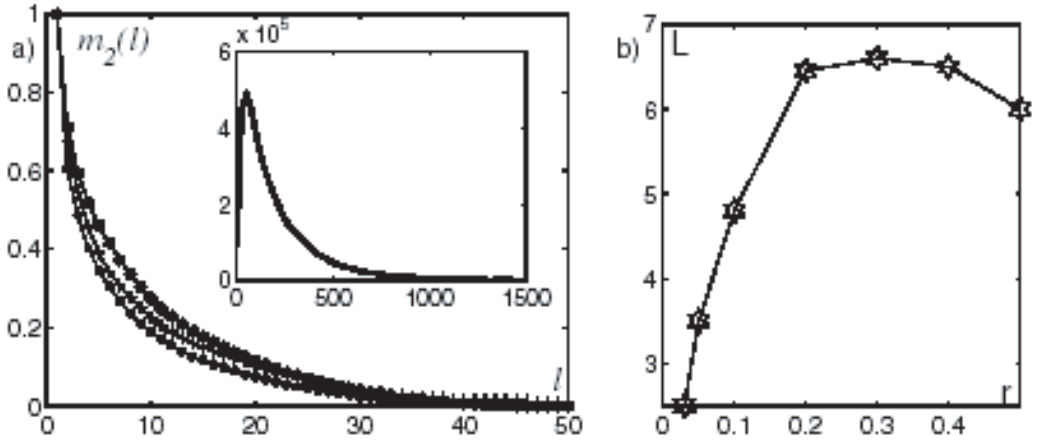

(a) (b)

Figure 16: Spatial heterogeneities (a) Second moment $m_2(\ell)$ of the relaxation time distribution, for different values of the cutoff distance $r[0.1(\bullet), 0.3(\star), 0.5(+)]$; the dependence of these curves on r is not monotonic (inset: relaxation time distribution for $r = 0.3$) (b) characteristic length L; it has a maximum L^* for $r = r^*$.

the curve of figure 16(b). L reaches a maximum of 7 particle diameters for $r = r^*$ which means that cage rearrangements are phenomena which imply more cooperation than the dynamics at other scales and that about a hundred particles are involved in such rearrangements. One then sees that cage rearrangements are highly cooperative phenomena. This, added to the small value of r^* shows that the picture of a particle escaping from a static cage formed by its nearest neighbours is over simplified.

Apart from precising the dynamics of the specific granular system presented here, this section also aimed at illustrating what can be done to characterise temporal and spatial correlations in systems in which one does not have access to the motion of all particles. In the same spirit, it is also possible to investigate some spatial correlations and discuss the existence of dynamical heterogeneities by considering multi-time correlation functions. However the analysis hardly leads to definitive conclusions and would lead us to discussions which are out of the realm of the present lecture. The reader who is interested can refer to the original work by Heuer et al. [40] and its application to the present system of interest by Marty et al. [54]. To obtain further evidences of the spatial correlations, and a better characterisation of the dynamical heterogeneities, one can no longer avoid to follow all particles. The next section will present the kind of analysis conducted in Saclay in the case of granular media, taking benefit of the bi-dimensional geometry of the set-up.

3.2.3 Spatial correlations and dynamical heterogeneities

The above sections 3.2.1 and 3.2.2 provided a "microscopic" confirmation of the similarity between glass and jamming transitions. The typical trajectories of grains display the so-called cage effect and are remarkably similar to the ones observed in experiments on colloidal suspension [68] and in molecular dynamics simulations of glass-formers [45, 46]. As for glass-formers, and contrary to standard critical slowing down, this slow glassy dynamics does not seem related to a growing *static* local order. For glass-formers it has been shown numerically [3, 41, 50, 8, 70] and experimentally [30] that instead the *dynamics* becomes

strongly heterogeneous and *dynamical correlations* build up when approaching the glass transition. Recent theoretical works [1] and the end of the previous section suggest that this also happens close to the jamming transition.

The aim of the present section is to present the analysis of the slow dynamics close to jamming measuring multi-point correlation functions as it has been done for super-cooled liquids [45, 46, 34, 29]. First, we shall focus on two point functions, in particular the intermediate scattering function and its self-part, whose slower than exponential relaxation suggests dynamical heterogeneity. Then we shall turn to four point correlation functions. They have been introduced for glass-formers to properly measure dynamical correlations [34, 29] and indeed reveal that the dynamics is strongly correlated and heterogeneous. Finally, we shall focus on spatio-temporal pattern of mobility, out of which we extract a direct measurement of a dynamical length-scale.

The second Saclay experimental setup 11(c) contains a bi-dimensional, bi-disperse granular material, composed of about 8.000 metallic cylinders of diameter 5 and 6 mm in equal proportions, which is again sheared quasi-statically in an horizontal deformable parallelogram. The shear is periodic, with an amplitude $\theta_{max} = \pm 5^\circ$. The volume accessible to the grains is maintained constant and the the volume fraction is $\Phi = 0.84$. In this set up, it is possible to follow 2818 grains (located in the center of the device to avoid boundary effects) with a High Resolution Digital Camera which takes a picture each time the system is back to its initial position $\theta = 0$. These conditions are very similar to those of the prototype and by repeating the same analysis the cage radius is found to be $r^* = 0.2$ and the cage lifetime $t^* = 300$.

The intermediate scattering function and its self part are commonly used in the literature when describing the structure and the dynamics of a liquid or a glass. We still recall here some useful algebra which will allow us to introduce a more general quantity – the density overlap – and give us the opportunity to introduce our notations. The very first quantity of interest is the instantaneous density field.

$$\hat{\rho}(r,t) = \sum_i \delta(r - r_i(t)) \tag{21}$$

where $r_i(t)$ is the position of the i^{th} particle at time t. One has that

$$\langle \hat{\rho}(r,t) \rangle = \bar{\rho} = \text{cst} \quad \text{and} \quad \int dr\, \hat{\rho}(r,t) = N \quad \text{hence} \quad \bar{\rho} = \frac{N}{V}. \tag{22}$$

Here and in the following, the hatted quantities denote the non average observable. In the experiment the average $\langle \cdot \rangle$ means a time average over 300 steps separated by 10 cycles each, taking care that on such time scales the processes are stationary. One then introduces a generalised density correlation function by considering

$$W_a(t) = \langle \hat{W}_a(t) \rangle = \frac{1}{N} \int dr dr' \langle \delta\hat{\rho}(r,t) w_a(r - r') \delta\hat{\rho}(r',0) \rangle, \tag{23}$$

where $\delta\hat{\rho} = \hat{\rho} - \bar{\rho}$ and $w_a(r - r')$ is some kernel with a space scale a to be precised later. Replacing $\hat{\rho}$ by its definition (21), one obtains after a small calculation:

$$W_a(t) = \frac{1}{N} \int dr dr' \sum_{i,j} \langle \delta(r - r_j(t)) w_a(r - r') \delta(r' - r_i(0)) \rangle - \bar{\rho} \int dr\, w_a(r) \tag{24}$$

$$= \frac{1}{N} \left(\langle \sum_{i,j} w_a(r_j(t) - r_i(0)) \rangle - < w_a >_V \right) \tag{25}$$

where $< . >_V$ is the mean value of the kernel function over the sample volume. The self part of this correlation function is given by considering only one particle, hence the same

formula replacing $r_j(t)$ by $r_i(t)$ and summing over one particle only. When considering the self part of such a correlation function, one obtains information about the single particle relaxation. When dealing with the non self correlation, one gains information about the structural relaxation. Using $exp(ik.r)$ for $w_a(r)$, where the space scale a is given by $2\pi/k$, $W_a(t)$ is nothing but the intermediate scattering function $F(k,t)$. When $w_a(r)$ is some overlap function decreasing from one in $r=0$ to zero for increasing r, $W_a(t)$ is called the density overlap correlation function, further noted $Q(a,t)$, as introduced by Franz and Parisi [34] and largely used by Donati et al. [29]. Practically, in the following computations $\delta(r)$ is approximated by a Gaussian of width 0.3.

The self part of the intermediate scattering function $F_s(k,t)$, where the subscript s here and in the following is for "self part", is plotted on the left of figure 17(a) as a function of time for different values of k ranging from 1 to 29. Contrary to glass-formers there is no visible plateau in this correlation function although from trajectories it was possible to identify a clear cage effect as seen in the previous section. A possible explanation is that the difference between the time-scales for the relaxation inside the cage and the escape from the cage is not large enough to give rise to a clear plateau. Except for very small k the decrease of $F_s(k,t)$ is slower than exponential in time. A good fit is provided by a stretched exponential: $\exp[-(t/\tau(k))^{\beta(k)}]$. We plot on the right of figure 17 $\tau(k)$ (top) and $\beta(k)$ (bottom) as a function of k. At small k the relaxation time scales as k^{-2} and the exponent $\beta(k)$ is one. As expected, the grains perform a Brownian motion on large length and time scales and therefore $F_s(k,t) \simeq \exp(-Dk^2t)$ for small k and large t [D is the self-diffusion coefficient of the grains]. Increasing k the stretched exponent decreases and is of the order of 0.7 for k of the order of 2π, corresponding to the inter-grain distance, and even lower for higher values of k. A very similar behaviour has been found in numerical simulations of glass-formers [45, 46]. Also the decrease of $\tau(k)$ steepens sharply for large k. This might be related to the sub-diffusive behaviour observed in the previous section : at short time the displacement distribution is roughly Gaussian with a variance varying as $t^{1/2}$ (not t like for standard diffusion). Hence, it would be natural that at large k the relaxation time went as k^{-4}. An overall very similar behaviour for the intermediate scattering function $F(k,t)$ (not plotted here) is obtained.

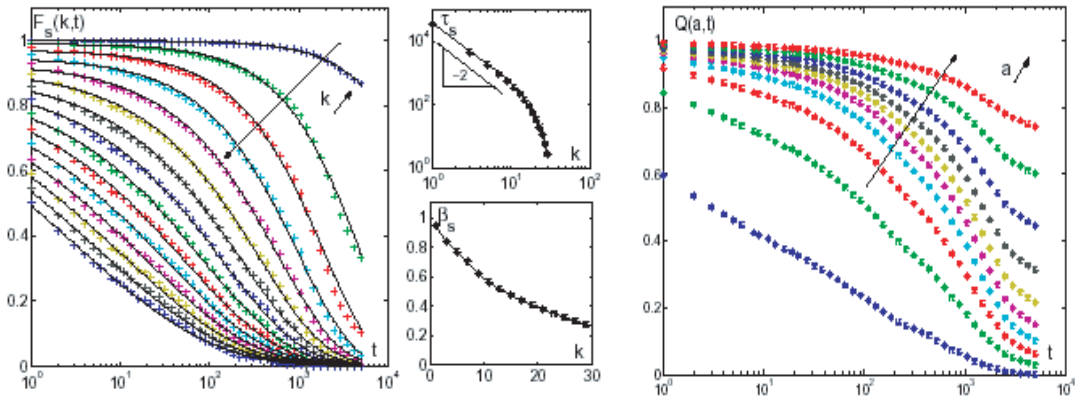

(a) (b)

Figure 17: Time correlations (a): $F_s(k,t)$ as a function of time for different values of the wave-vector $k = 1,3,...,29$. The black lines represent fits of the form $\exp[-(t/\tau(k))^{\beta(k)}]$; on the right: $\tau(k)$ (top) and $\beta(k)$ (bottom) as a function of k. (b): $Q_a(t)$ as a function of time for $a = 0.05, 0.1, ..., 0.5$.

Dynamical heterogeneity is one of the possible explanation of the non-exponential relaxation of $F_s(k,t)$ (and of $F(k,t)$): the relaxation becomes slower than exponential because there is a wide spatial distribution of time-scales [30]. However this is not the only possible scenario [20, 30]. In the following we want to go one step further and show direct "smoking gun" evidences of dynamical correlations. The proper way to unveil these correlations is through the fluctuations of the correlations [34]. The idea is that the temporal correlation is itself the order parameter of the transition. Accordingly, its fluctuations should unveil correlations exactly as fluctuations of the magnetisation unveil magnetic correlations close to a ferromagnetic transition. These fluctuations are characterised by four points correlation functions generically defined as:

$$\chi_4^W(t) \quad = \quad N\langle\left(\hat{W}_a(t) - \langle\hat{W}_a(t)\rangle\right)^2\rangle \tag{26}$$

where W_a can be the intermediate scattering function, the density overlap, or their self part. It happens that the complex exponential kernel used to construct the intermediate scattering function -historically justified by the light scattering experiments- induces artificial fluctuations which prevent from properly computing the corresponding χ_4. From that point of view, the density overlap is much more convenient. Figure 17(b) displays $Q(a,t)$, where the overlap function $w_a(r)$ has been chosen as a non-normalised Gaussian: $w_a(r) = \exp(-r^2/2a^2)$. The evolution of $Q^a(t)$ is a measure of how long it takes for the systems to de-correlate from its density profile at time $t = 0$. One can verify that the behaviour of $Q(a,t)$ is very similar to that of $F_s(k,t)$, as for glass-formers [34, 50].

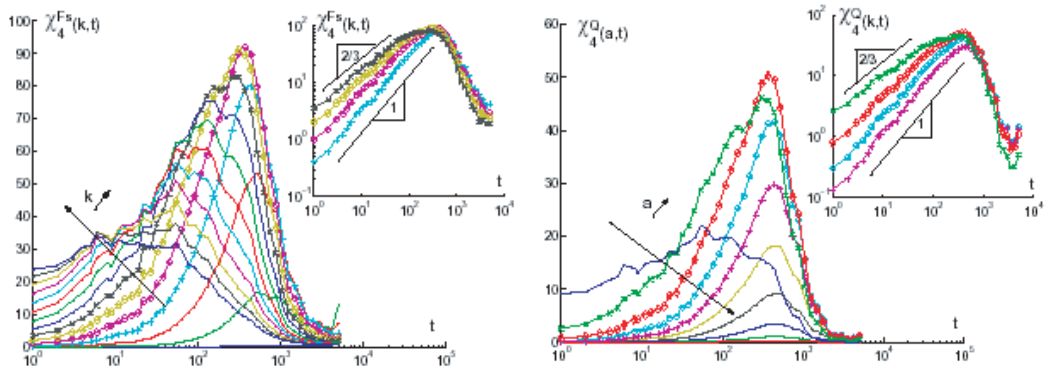

Figure 18: Four-points correlations (a):$\chi_4^{F_s}(t)$ as a function of time for values of $k = 1,3,...,29$. Inset: Log-Log plot for $k = 7,9,11,13$. (b):$\chi_4^Q(t)$ as a function of time for values of $a = 0.05,0.1,...,0.5$. Inset: Log-Log plot for $a = 0.1,0.15,0.2,0.25$.

Figure 18(a) displays $\chi_4^{F_s}(t)$ for $k = 1,3,...,29$. It has the form found for glass-formers [3, 50, 8, 70, 67]: it is of the order of one at small and large times and displays a peak at a time somewhat larger than the cage lifetime. The largest $\chi_4^{F_s}(t)$ is obtained for $k = 9$ corresponding to a length of the order of the cage size. The behaviour at small and large times is in a sense expected since in these limits $\chi_4^{F_s}(t)$ can be related to static correlation functions, which, as discussed previously, do not show any long range order. Alternatively the peak is a clear signature of dynamic heterogeneity and shows that the dynamics is maximally correlated on time-scales of the order of the relaxation time. A rough estimation of the corresponding dynamical correlation length is obtained by identifying the peak of $\chi_4^{F_s}(t)$, of the order of 100, to a correlated area $\pi\xi_{het}^2$, leading to a length $\xi_{het} \propto 6$ in agreement with

the estimate of the previous section. Very similar results are found for $\chi_4^Q(t)$ as shown in figure 18 for $a = 0.05, 0.1, ..., 0.5$. It is interesting to note that, as found for glass-formers in [50], the main contribution to $\chi_4^Q(t)$ comes from the fluctuations of the self-part of Q. Indeed we checked that for small and intermediate a, $\chi_4^Q(t) \simeq \chi_4^{Q_s}(t)$ and only for $a > 0.25$ one starts to see a difference. The growth of $\chi_4^{F_s}(t)$ (resp. $\chi_4^Q(t)$) before the peak seems to follow a power law with an exponent which depends on k (resp. a) and varies between 1 and $2/3$. As discussed in [67] the form of $\chi_4^{F_s}$ and χ_4^Q provides interesting information on the mechanism behind dynamical heterogeneity. Such power law behaviours with exponents between 1 and $2/3$ suggest that the dynamic correlations cannot be induced by independent defects or free volume diffusion [67].

It would now be very interesting to have some insight on the spatial origin of the fluctuations evidenced by the computation of $\chi_4(t)$. One way to understand how these fluctuations relate to spatial heterogeneities of the dynamics is to decompose, say, $Q(a,t)$ in local contributions: $N\hat{Q}(a,t) = \rho \int dr \hat{q}_a(r,t)$ where $\hat{q}_a(r,t) = 1/\bar{\rho} \int dr' \delta\rho(r,t) w_a(r-r') \delta\rho(r',0)$.

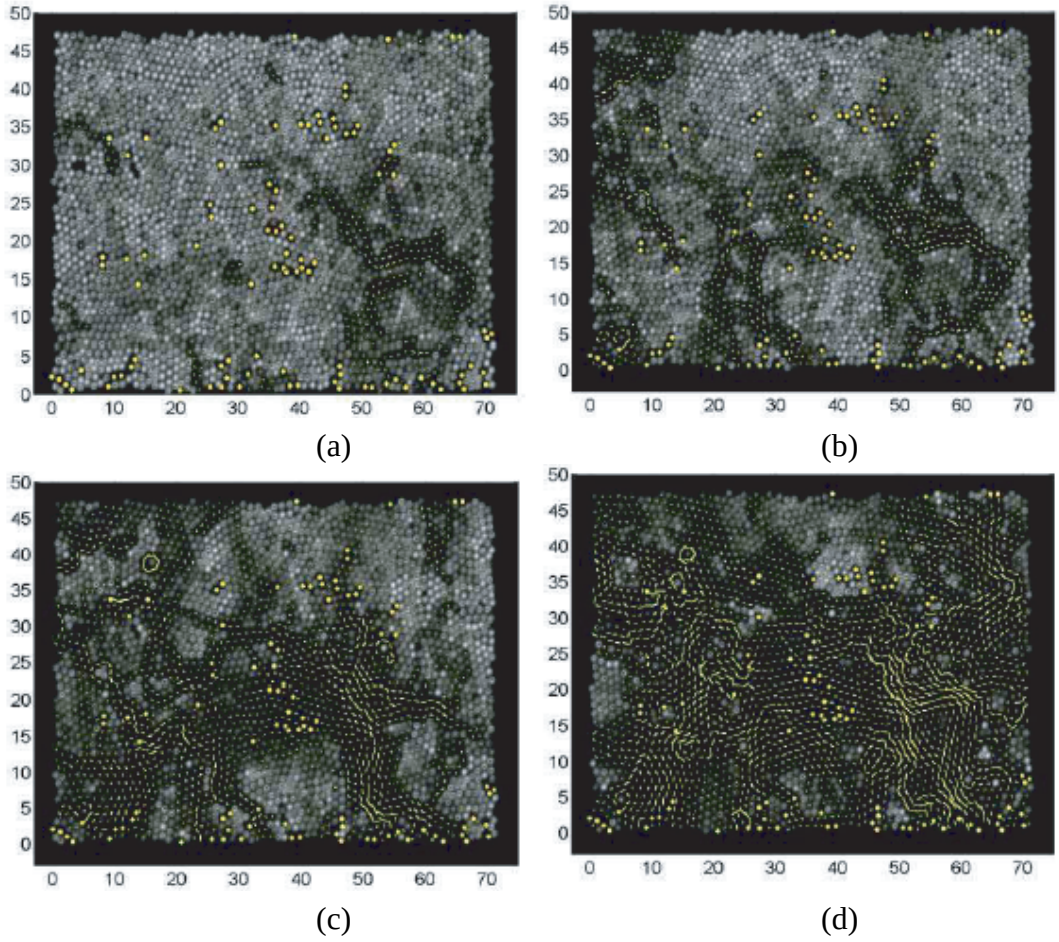

Figure 19: Grey-scale plot of $\hat{q}_{a_S}(r,t)$, at $t = 154, 435, 1113, 2526$ from top to bottom in a grey-scale ($a = 0.15$). Black regions correspond to lower values of $\hat{q}_{a_S}$. The displacements of the particles during the interval of time t are plotted in yellow. The yellow dots are particles that have been lost during tracking.

Using this last expression one finds that $\chi_4^Q(t) = \rho \int dr G_4^Q(r,t)$ where $G_4^Q(r,t) = \langle [\hat{q}_a(r,t) - \langle \hat{q}_a(r,t) \rangle][\hat{q}_a(0,t) - \langle \hat{q}_a(0,t) \rangle] \rangle$. This last expression states that $\chi_4^Q(t)$ is nothing but the mean value over the sample of the spatial correlations among the local temporal correlation.

It clearly shows that a large value of $\chi_4^Q(t)$ has to be related to long range spatial correlations of $G_4^Q(r,t)$, which is the spatio-temporal representation of the local temporal correlations.

Figure 19 presents a grey-scale plot of the self-part $\hat{q}_{as}(r,t) = \sum_i \delta(r - r_i(0)) w_a(r_i(t) - r_i(0))$ for $t = 154, 435, 1113, 2526$ and $a = 0.15$. By definition $\hat{q}_{as}(r,t)$ measures in a coarse grained way the local mobility: if the particle that was close to r at $t = 0$ moved away more than a in the time interval t then $\hat{q}_{as}(r,t) \simeq 0$. The yellow lines in figure 19 are the particle displacements in the time interval t. The four chosen time intervals correspond from top to bottom to short-times, relaxation times, moderate long times, long-times. At short-times ($t = 154$) only few particles have moved and from figure 19 it appears that they do so in a string-like fashion. On larger times ($t = 435, 1113$) the relaxed regions are ramified and finally, at very long time ($t = 2526$) the overall majority of the particles has moved substantially but there remain few (rather large) regions not yet relaxed. These findings, similar to the ones found in simulation of super-cooled liquids [3, 50] and experiments on colloidal suspensions [69] suggest that the mobility is organised in clusters, which are the direct visual evidence of the dynamical heterogeneities.

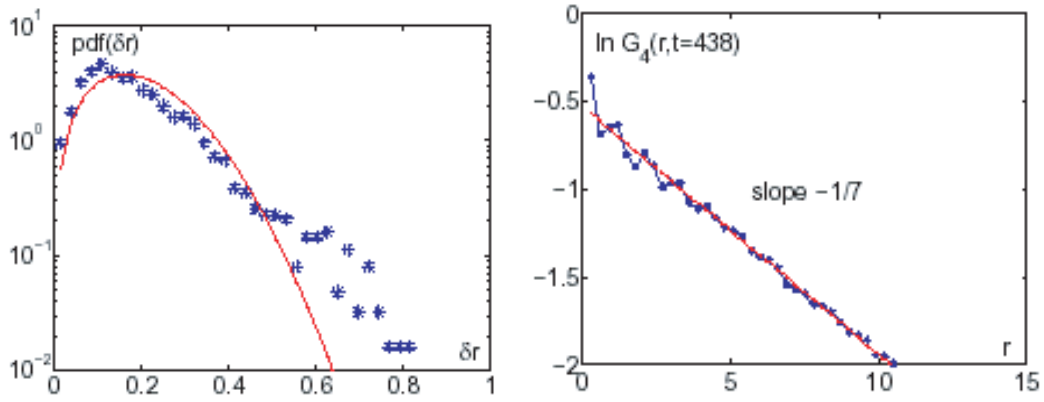

(a) (b)

Figure 20: (a): Self part of the Van Hove correlation function after angular integration at $t = 438$; the continuous line is the pdf obtained assuming a Gaussian distribution. (b): $\ln(G_4(r,438))$ as a function of r; the straight line is a linear fit.

To further quantify the heterogeneities, we estimate how large is the mobility difference between fast and slow grains. Figure 20(a) displays the self part of the Van-Hove correlation function, i.e. the probability distribution of the grains displacements amplitudes for $t = 438$ (corresponding to the maximum of $\chi_4^Q(t)$). It clearly demonstrates the excess of fast and slow grains compared to the distribution obtained when assuming a Gaussian process (in continuous line). The fast grains are roughly five time faster than the slow ones. Furthermore, we obtain $G_4(r,438)$ by computing the radial autocorrelation of $\hat{q}_{as}(r,t)$, and averaging over ten realizations. Figure 20(b) shows that $G_4(r,438)$ decays exponentially over a characteristic dynamical length $\xi = 7$, in agreement with the value obtained from the peak of $\chi_4^{F_s}$.

3.3 Partial Conclusion

In this second part of the lecture, we have seen that the analogy observed at the macroscopic level between dense granular media close to the jamming transition and super-cooled liquids close to the glass transition has indeed microscopic grounds. Despite the difference in the

driving mechanisms – a mechanical instead of a thermal forcing –, the diffusion properties of a single particle and the collective relaxation of the system share very strong similarities including the existence of a dynamical length increasing at the transition.

At the root of these very strong similarities is the physical nature of the transition. In the case of thermal systems close to the glass transition, the dynamics is dominated by the complex shape of the multidimensional potential energy landscape. The thermal activation being weaker and weaker, the system spend more and more time in meta-stable states. Eventually the system does not equilibrate on experimental time scales and falls out of equilibrium. In the case of the dense granular systems under gentle forcing, the grains rearrange among mechanically stable configurations which are the equivalent of the meta-stable states. When the external forcing is decreased, or when the density is increased, the grains rearrangements become more and more difficult to produce. In both cases, the relaxation evolves towards a global structural relaxation involving collective behaviours and characterised by dynamical heterogeneities.

As a matter of fact, the analogy is so strong that the glass transition can be seen as a specific case of jamming transition as suggested by Liu and Nagel [52]. The interest of such a unifying view is double. First, as we shall see in the last part of the present lecture, theories developed in the field of glasses have inspired interesting development in the field of granular media. Second, as we saw in this part, granular media can be seen reciprocally as a very convenient experimental system for studying the microscopic features of the structural relaxation close to the glassy state.

4 Looking for a statistical description

As just stated, one of the key ingredients of the non-trivial phenomenology observed in both granular media and thermal glasses is the large number of microscopic meta-stable states, among which the system hops during its slow dynamical evolution. In the context of glassy systems, Stillinger et al. [65, 66], introduced the concept of inherent structures, namely the potential local minima. Following the ideas of Goldstein [36], the phase space trajectory of the system can be described as successive steps among the potential basins. The entropy is then claimed to be separable into one vibrational part accounting for the vibrational modes around the minima and one configurational part accounting for the numerous inherent structures. In the thermodynamical analogy proposed by Edwards [33], that we will discuss in the following, the mechanically stable states of a granular packing are given a similar role to that of the inherent states and called ”blocked states”.

The natural question that immediately arises is that of the weight of these configurations in a given experiment and how they encode the specificity of the dynamics. Various forms of the fluctuation-dissipation relation have been generalised to out of equilibrium situations of thermal systems by Cugliandolo, Kurchan and collaborators [18, 19]. Such generalisations lead to the definition of an effective temperature for the long-time behaviour of glassy systems. The existence of such an effective temperature suggests for these systems some kind of ’ergodicity’ in the dynamics among the meta-stable states. Extending these ideas to the case of granular media as suggested by Kurchan [48, 49] may provide some validity to Edwards’ assumption that all blocked configurations in the jammed state are equiprobable leading to the so called ”Edwards’ ensemble”.

However the situation is far from being clear. Let us recall some of the remarks made by Bouchaud [12] in his lecture in Les Houches, to motivate the last part of the present lecture:

- Despite phenomenological analogies between temperature and gentle tapping, one

should keep in mind that tapping is a long-wavelength excitation, whereas temperature is thought to give rise to very short wavelength excitation. Accordingly detailed balance and activated process ideas might need to be reconsidered.

- The choice of the microscopic variables is already not obvious. Also, dealing with continuous variables such as the contact forces for instance, one has to assume the uniformity of the a priori measure on the forces as done on the canonical variables (position and momentum) when building the microcanonical ensemble for particles. However, in the latter case, the procedure is justified by the Liouville theorem resulting from the Hamiltonian dynamics. In the case of granular media no physical prescription has been proposed yet.

In this part, we will present Edwards' proposal, discuss how and whether they can be tested experimentally and finally produce some recent results on free volume statistics inside a bi-dimensional granular packing.

4.1 Edwards' proposal

In the statistical physics of Hamiltonian systems [51, 25], the microscopic configurations $\mathscr{C}$ are described by the canonical variables prescribed by the Liouville's theorem, the momenta and positions $\mathscr{C}(p_i,q_i)$ of all particles. In the case of an isolated system with total energy E, one obtains as a stationary state of the Liouville's equation, a uniform equilibrium probability density over the micro-states of energy E. Accordingly for a system defined by its Hamiltonian $H(p_i,q_i)$:

$$P(\mathscr{C}(p_i,q_i)) = \frac{1}{\Omega(E)}\delta(H(p_i,q_i)-E) \quad \text{with} \quad \Omega(E) = \int \prod_i dp_i dq_i \delta(H(p_i,q_i)-E). \tag{27}$$

The entropy at equilibrium and the temperature are then given following the construction presented in section 2.2 by:

$$S(E) = -\sum_{\mathscr{C}} P(\mathscr{C})\ln(P(\mathscr{C})) = \ln\Omega(E) \quad \text{and} \quad \beta = \frac{1}{T} = \frac{\partial \ln\Omega(E)}{\partial E}. \tag{28}$$

Behind this very elegant formalism stand a few but essential properties of Hamiltonian systems. We have already mentioned the prescription for the appropriate microscopic variables (p_i,q_i), by the Liouville's theorem, which derives itself from the canonical structure of the equations of Hamilton. One must also consider the symmetries such as the time reversal and the time translational invariances, the latter giving rise to the conservation of energy. Finally, assuming that the uniform distribution is the true distribution of the system is given by the ergodic hypothesis.

Consider now a granular media close to the jammed state. In Edwards' description [33, 31, 32], it is first assumed that the volume $\mathscr{V}$ is the key macroscopic quantity governing the behaviour of the system. Then, it is assumed that the statistics is completely dominated by the "blocked configurations", which are claimed to all have the same statistical weight. Hence the probability of a configuration $\mathscr{C}$ in a system of fixed volume V is:

$$P(\mathscr{C}) = \frac{1}{\Omega(V)}\Theta(\mathscr{C})\delta(V(\mathscr{C})-V) \quad \text{with} \quad \Omega(V) = \int d\mathscr{C}\Theta(\mathscr{C})\delta(\mathscr{V}-V). \tag{29}$$

where $\Theta(\mathscr{C})$ is a constraint to restrict the configurations to the "blocked states". An analogous entropy and the corresponding analogue of the temperature, named the "compactivity"

are then given by

$$S(V) = -\sum_{\mathscr{C}} P(\mathscr{C}) \ln(P(\mathscr{C})) = \ln \Omega(V) \quad \text{and} \quad \frac{1}{X} = \frac{\partial \ln \Omega(V)}{\partial V}. \tag{30}$$

Given the very strong properties of the Hamiltonian systems which support the equilibrium statistical description, Edwards' proposal looks at first sight a rather crude analogy and at least calls for a few comments.

- Let us discuss first the choice of the volume. It is a natural extensive macroscopic quantity and it clearly plays a crucial role in the rearrangements of the grains among jammed configurations. However, it should be shown that it is conserved by the dynamics, a key ingredient for the above construction as illustrated in the first part of this lecture. The total volume accessible to the grains can be fixed, such as in the shear experiment conducted in Saclay. Assuming then some tiling of the space accessible to the grains in a given experiment, the grains rearrangements can be described by a redistribution of the volume among the grains. In this sense, there is indeed a local conservation of the volume. Even if the total volume is not fixed, as in most tapping experiments, on can check that the system is large enough to ensure sufficiently small fluctuations of its volume. In such a case, provided that the grains rearrangements do not cascade to the free surface of the packing, the system can serve as a reservoir of volume for a sub-system, which then has to be described in the canonical formalism. Yet, one sees that one important hypothesis is to have enough local redistribution of the volume.
- The choice of the microscopic variables, as already mentioned, is extremely ambiguous. There is no general prescription neither for the minimal list of relevant physical quantities, nor for the choice of the appropriate variables to describe them. Ignoring physical quantities will falsify the computation of the density of states. Having no prescription for the correct choice of variables induces an irreducible ambiguity since the uniform measure for continuous variables is not conserved under a change of variables.
- Time reversal symmetry and the ergodic hypothesis are crucial for assuming a uniform distribution among the accessible configurations. Given the existence of dissipation and the very slow compaction of granular media under gentle tapping there is little chance to observe time reversal symmetry in the general case. Furthermore, even for a stationary dynamics, checking the existence of micro-reversibility in a real system, is out of reach of experimental investigations.

Altogether Edwards' description is a challenging proposal, the implementation of which is far from being obvious and which calls for experimental and numerical validations. Despite some clear examples where Edwards approach fails [35], various checks have been made so far in mean field models of the glass transition [55], in schematic finite-dimensional models with kinetic constraints [4, 5], in spin glass models with a-thermal driving between the blocked states [24] and finally in a few more realistic models of particle deposition [14] or MD simulations of shear driven granular media [53]. Reviewing these studies is out of the scope of this lecture. It should be stated however that in most of these works, the accent is put on the validation of the uniform measure over the blocked states. A given model being chosen, its dynamics is computed at constant volume. Blocked states are identified and dynamical averages of macroscopic quantities are compared with averages over the blocked states assuming equal weights. The issue of the proper choice of variables to describe a granular media is not considered. Finally most of these models use Monte-Carlo algorithm

to generate the dynamics so that implicitly, the dynamics is reminiscent of an Hamiltonian kind of dynamics. In the last section, we will discuss what can be tested experimentally in Edwards' proposal and present recent results obtained in this direction.

4.2 Experimental test of Edwards' proposal?

4.2.1 Volume fluctuations

Formula (29) gives the probability of a given configuration of volume V, according to Edwards' proposal. In order to investigate its validity, let us assume that the probability distribution over the blocked configurations is *not* uniform, but given by a density $f(\mathscr{C})$. Formula (29) then turns into:

$$P_\mu(\mathscr{C}) = \frac{1}{Z_\mu(V)} f(\mathscr{C})\Theta(\mathscr{C})\delta(V(\mathscr{C})-V) \quad \text{with} \quad Z_\mu(V) = \int d\mathscr{C}\, f(\mathscr{C})\Theta(\mathscr{C})\delta(V(\mathscr{C})-V) \tag{31}$$

As for usual thermodynamics, it is uneasy to study an isolated system since the experimentally measurable quantities of interest are then fixed from the outside. The usual way to proceed is to consider a subsystem, free to exchange volume with a reservoir, that is a system in the canonical situation. We have seen in the first part of this lecture, section 2.2, equation (12), that, *provided that both* $f(\mathscr{C})$ *and* $\Theta(\mathscr{C})$ *factorize for any partition of the system*, the canonical probability distribution can be written :

$$P_c(\mathscr{C}) = \frac{1}{Z_c(X)} f(\mathscr{C})\Theta(\mathscr{C}) \exp -(V(\mathscr{C})/X) \quad \text{with} \quad \frac{1}{X} = \frac{\partial \ln Z_\mu(V)}{\partial V}\Big|_{V^*}, \tag{32}$$

where V^* is the most probable value of the volume of the reservoir.

This probability distribution is still out of reach of experimental and even numerical investigations, since it requires to sample all microscopic configurations. However, as seen in section 2.2, equation (15), the usual thermodynamical equalities remain valid, so that the fluctuations of the volume can be related to the average volume by:

$$\langle V^2\rangle - \langle V\rangle^2 = X^2 \frac{\partial \langle V\rangle}{\partial X}. \tag{33}$$

Inverting this relation, one can in principle extract from the simultaneous measure of $\langle V\rangle$ and $\langle V^2\rangle$ the dependance of the compactivity on the volume $X(V)$. This is precisely what has been done by Schröter et al. [62] in the Austin experimental set-up presented on figure(3d) and that we will now discuss in more details.

In their work Schröter et al. [62] use a periodic train of flow pulses in a fluidized bed. A column of glass beads in water is expanded by an upward stream of water until it reaches a homogeneously fluidized state, and then the flow is switched off. The fluidized bed forms a sediment of volume fraction Φ, which depends in a reproducible way on the flow rate of the pulse. This forcing results in a history independent steady state where the volume exhibits Gaussian fluctuations around its average value. The history independence is demonstrated by ramping up and down in flow rate ; both the averaged volume fraction Φ_{avg} and the standard deviation σ_Φ depend only on the flow rate of the last flow pulse, not the earlier history of the bed.

As shown on figure 21(a) the variation of σ_Φ with Φ_{avg} is well fitted by a parabola with a minimum for some specific value of the averaged volume fraction. Relating this minimum of the fluctuations to a maximum in the number of statistically independent spatial regions at the moment of solidification, the authors suggest the following explanation. For smaller volume fraction, the sample is more fragile and local rearrangements induce large

reorganisations. For larger volume fraction, the free volume becomes smaller, the system is more jammed and any local rearrangement requires a large reorganisation of the packing.

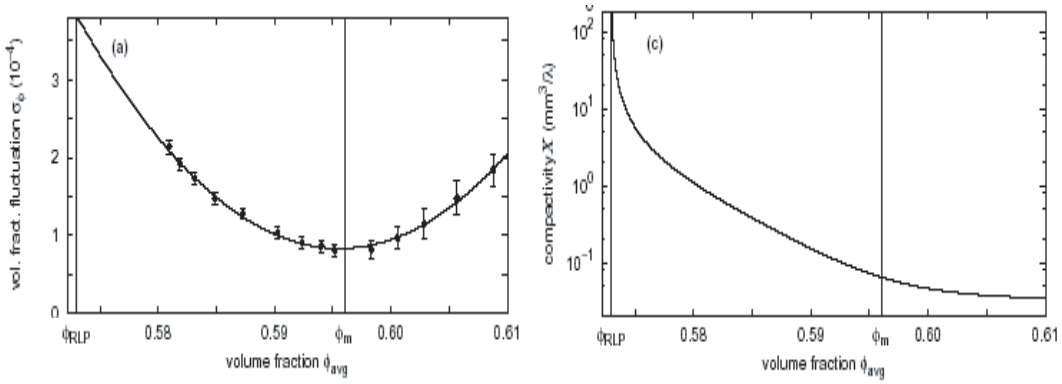

(a) (b)

Figure 21: Fluctuations and compactivity in Austin experiment (a): Volume fluctuations as a function of the mean volume. (b): Compactivity as a function of the mean volume.

Using the relation (33), the authors derive the following relation

$$\frac{\lambda\rho}{m}\int_{\Phi_{RLP}}^{\Phi} d\phi \left(\frac{\phi}{\sigma_\phi}\right)^2 = \frac{1}{X(\Phi)} \tag{34}$$

where it has been assumed in the spirit of Edwards' proposal that $X(\Phi_{RLP}) = \infty$ and that Φ_{RLP} is obtained in the limit of very large flow rate. Note that in the present lecture λ, the equivalent of the Boltzmann constant, has been fixed to one. This relation leads to the dependance of the compactivity X on the averaged volume fraction Φ_{avg} displayed on figure 21(b).

The above results are the very first experimental measurements of the so-called compactivity. Unfortunately, in the absence of a theoretical prediction for the dependence of the compactivity on the volume, they do not check Edwards' proposal in anyway. As a matter of fact, for any system, in any situation, it is always possible to first measure the averaged value and the fluctuations of any given macroscopic observable V, then *define* X assuming a thermodynamical relation such as (33) and obtain $X(V)$.

4.2.2 Free volume distributions

To go one step further, one might think of investigating the full probability distribution of the volume, not only at the scale of the packing but for subsystems of increasing sizes. From the canonical probability distribution (equation 32), one readily computes the probability of observing a volume V in a subsystem of N grains:

$$P_c(V_N) = \int d\mathscr{C} P_c(\mathscr{C})\delta(V(\mathscr{C}) - V_N) = \frac{Z_\mu(V_N)}{Z_c(X)} \exp -V_N/X, \tag{35}$$

Apart from the exponential weight, most of the information about the system lies in the pre-factor dependance on V_N. Hence, one crucial step to go further is to precise what are the variables which describe the microscopic configurations. Given the role played by the volume, it could be natural to consider the volumes w_i associated to each grain through some tiling of the space, as suggested by Edwards. However, it is clear that the choice of such

a set of variables is not sufficient since it does not include the forces at the contacts. As a consequence one will have to include a density of state $\rho(w_1, w_2, ..., w_N)$ in the description and the microcanonical partition function will read:

$$Z_\mu(V_N) = \int \prod_i dw_i \rho(w_i) f(w_i) \Theta(w_i) \delta(\sum_i w_i - V_N). \tag{36}$$

One already sees that without a theoretical prescription for the density of states ρ, a formidable task to achieve, there is little chance to test the measure $f(w_i)$. Let us take an example to make this last point more precise. Consider a system for which $f(w_i) = \prod_i w_i^{\eta-1}$ [10, 11] and for which $\rho(\lambda w_1, \lambda w_2, ..., \lambda w_N) = \lambda^{\gamma N} \rho(w_1, w_2, ..., w_N)$. Then introducing the adimensionalized volumes ω_i defined by $w_i = \omega_i V_N/N = \omega_i v_N$, one obtains:

$$Z_\mu(V_N) = (V/N)^{N-1} (V/N)^{\gamma N} (V/N)^{N(\eta-1)} \int \prod_i d\omega_i \rho(\omega_i) \Theta(\omega_i) \delta(\sum_i \omega_i - N), \tag{37}$$

and thereby

$$P_c(v_N) = \frac{A(N)}{Z_c(X)} v_N^{(\gamma+\eta)N-1} \exp -N v_N/X. \tag{38}$$

This last expression shows clearly that the details of the microcanonical measure (here the value of η) cannot be distinguished from the specific properties of the density of state (here the value of γ). In particular the uniform measure ($\eta = 1$) does not emerge as a special case.

However, the microscopic physics of the system remains fully embedded in the microcanonical partition function and therefore, it is still of interest to investigate its shape and in particular to evaluate its dependence on the system size. This task has been conducted by Da-Cruz et al. [17] in the case of a bi-dimensional packing. The experimental set up (Fig. 22a) consists in a rectangular glass container which contains 5000 nickel plated brass cylindrical spacers of two different diameters $d_s = 4$mm and $d_l = 5$mm in equal number. In the following d_s has been chosen as the unit length. The cell is half filled with a single layer of such hard disks mixed together, resulting in an homogeneous and disordered bi-dimensional packing. The cell is mounted on a horizontal axis and rotated around this axis in such a way that the grains fall from one side to the other every half cycle. The experimental procedure is the following. The cell starts in a vertical position and is rotated one cycle, at a constant speed of one cycle per minute. During this cycle, the grains fall from one side to the other and then back to the initial side. The engine is stopped, the system allowed to reach a mechanically stable state, and a picture of the bulk is taken. 15 000 of such cycles are performed. The pictures hence taken display on average 300 grains. For each picture the centers of the spacers are located and their Voronoi diagram is computed (Fig 22b), taking into account the bidispersity of the assembly. One then collects the area of the cells along with the type, position and index of the associated grains. Out of these raw data, the statistical distribution of the free volumes occupied first by one grain, then by clusters of an increasing number of neighbouring grains are extracted and analysed.

Figure 22(b) displays the distribution of the Voronoi cell areas. The distribution displays two peaks centered on $< v_s >= 1.00$ (resp. $< v_l >= 1.49$), the averaged area occupied by the small, (resp. the large) grains computed independently. Also indicated on the figure are the minimal values that a Voronoi cell can possibly take - the closest regular hexagon- for each type of grain, $v_s^{min} = \sqrt{3}/2 \simeq 0.866$ and $v_l^{min} = \sqrt{3}/2(d_l/d_s)^2 \simeq 1.35$. Both peaks present a well defined exponential tail, which is easily isolated when considering the distributions of the free volume ($v_{s,l}^f = v - v_{s,l}^{min}$), for each type of grain as shown on the inset of figure 22(b). Note that these exponential tails and the associated characteristic free volumes should not

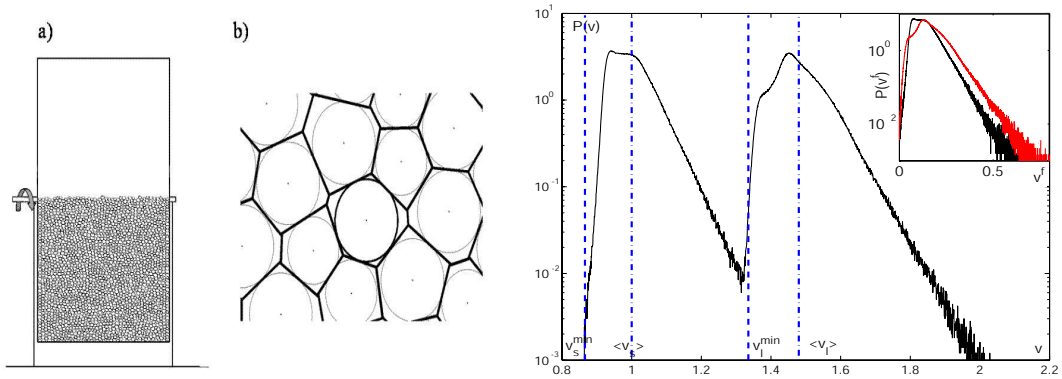

Figure 22: (a) Experimental set-up and sketch of the modified Voronoi tessellation; (b) Distribution of the Voronoi cells area. Vertical dashed lines : minimal Voronoi cell area. Vertical dash-dotted lines : conditional average Voronoi cell area. Inset: distributions of the free volume conditioned by the grain size; (dark): small grains; (grey): large grains

be interpreted as a signature of the Gibbs weight, and thereby as some kind of validation of Edwards' hypothesis as sometime suggested in the literature. At least one should consider larger subsystems.

Accordingly, let us turn to the free volume distributions for clusters of neighbouring grains. Figure 23(a) displays the distribution of the free volume per grain inside clusters of N neighbouring grains, $v_N^f = N^{-1}\Sigma_{i=1}^N v_i^f$. The authors choose to describe the distributions of the free volume per grain inside a cluster of N neighbouring grains by a Gamma law of parameters η_N and X_N as suggested by the the shape of the distributions, the example discussed here above and the expected convergence towards the gaussian law :

$$P(v_N^f) = \frac{1}{X_N^{\eta_N}\Gamma(\eta_N)}(v_N^f)^{\eta_N-1}e^{-v_N^f/X_N}. \tag{39}$$

where Γ is the Euler Gamma function. Once chosen the form of the distributions, one computes their first two moments and obtain η_N and X_N, through the relations $< v_N^f >= \eta_N X_N$ and $< {v_N^f}^2 > - < v_N^f >^2 = \eta_N {X_N}^2$. As expected, $< v_N^f >$ rapidly evolves towards a constant (figure 23(b)-top). On the contrary $< {v_N^f}^2 > - < v_N^f >^2$ varies like $N^{-\alpha}$ with $\alpha = 0.75 \pm 0.0025$, in contrast with the $1/N$ dependence expected for independent variables (figure 23(b)-bottom). Altogether, the distribution of the free volume per grain inside clusters of N grains is well described by a Gamma law, the parameters of which exhibit the following dependences on N : $\eta_N = \eta_{eff} N^{\alpha}$ and $X_N = X_{eff} N^{-\alpha}$, with $\eta = 3.5$ and $X = 0.041$.

Altogether, rewriting the above Gamma law in the limit of large N, one obtains that the logarithm of the distribution of the free volume per grain inside clusters of N grains scales as $N^{\alpha} g(v, \eta_{eff}, X_{eff})$ with $g(v) = \eta(\ln(v/(\eta X)) - v/(\eta X) + 1)$, $\alpha \simeq 3/4$, $\eta_{eff} \simeq 7/2$ and $X_{eff} = 0.041$. Finally, one can also write the distribution of the free volume per grain inside clusters of N grains as:

$$P(v) = \frac{1}{Z(N,\eta,X)} e^{-N^{\alpha}\left(\frac{v}{X} - s(v)\right)}, \quad \text{with} \quad s(v) = \eta \ln(v), \tag{40}$$

and thereby $\frac{1}{X} = \frac{\partial s}{\partial v}\Big|_{\langle v \rangle}$, an exact result given the Gamma law distribution and more generally expected from a saddle point calculation in the large N limit.

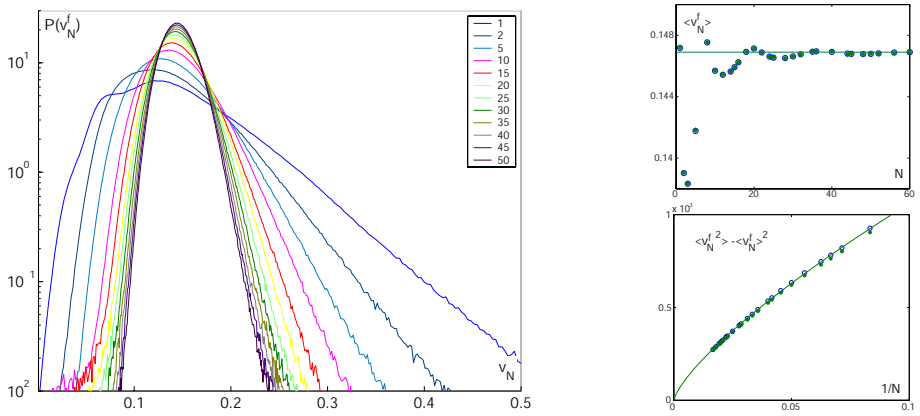

(a) (b)

Figure 23: Free volume statistics. (a): distributions of the free volume per grain inside clusters of N grains; the larger N, the narrower the distribution. (b): dependence on N of the first (top) and second (bottom) moments of the free volume distributions ($\circ$): computed from the data; ($*$): extracted from the fit of the distributions by a Gamma law; (plain line): fit of their dependence on N

This central result deserve a few comments : First, the observed non extensive factor N^{α} is presumably the evidence of long range correlations between the free volumes of individual grains. Indeed, in the presence of correlations decaying with the distance r as $1/r^{\gamma}$, one has in two dimensions, for $\gamma < 2$, that the second moment of the average of N centered random variable scales like $N^{-\gamma/2}$. In the present case, we would thus infer the existence of long range correlations decaying like $1/r^{3/2}$. If the existence of such long range correlations is confirmed, then the thermodynamical description will have to take them into account in order to define properly the extensive and the associated intensive parameters. For instance, the use of the relation (33) as done by Schröter et al. leads to the definition of a compactivity, which depends on the system size! Also, the existence of such long range correlations may invalid the hypothesis of a local conservation of the volume. Second the above analysis has allowed to define two effective parameters which characterise the probability distribution of the free volume for one grain. How do they relate to Edwards' compactivity? Do they equilibrate between subsystems put into contact? Is it still possible to define a thermometer in the most general sense? Many questions remain open.

To conclude this part, testing Edwards hypothesis appears to be extremely challenging. Whereas much of the focus is usually put on the uniformity assumption for the probability distribution of the blocked states, we have seen here that in practice it is hard to distinguish it from another factorizable distribution, until one has a full microscopic description of the systems and its dynamics. Conversely, a lot can be learned from the investigation of the probability distributions of various macroscopic variables. It is of major interest to understand how many intensive parameters are necessary to describe these distributions and whether they equilibrate between subsystems in contact. Identifying these parameters would be a major step in the thermodynamical description of granular systems.

5 Conclusion and perspectives

In this lecture we have tried to discuss both theoretical ideas and experimental results on the thermodynamics of granular media and its statistical grounds. After having precised the concepts of thermal vs. a-thermal systems, we have reviewed the experimental evidences of the strong similarities between the granular media close to the jamming transition and super-cooled liquids close to the glass transition, at both the macroscopic and the microscopic scale. Finally, we have discussed in details Edwards' proposal for a statistical description of jammed granular media and illustrated the kind of experimental study, which are conducted in this spirit.

As recalled in the introduction, the understanding of granular media and a-thermal systems in general is far from being completed. Many of the ideas exposed here will change; many experimental results will find new interpretations. Let us still stress one more time, what we believe are the main messages of this lecture in the present state of knowledge.

In the first part, it was shown that the definition of a temperature or an equivalent is actually not related to the scale of the particles, but to the existence of an extensive conserved quantity. In the second part, it has been observed that the idea of a unified description for the glass and the jamming transition has indeed strong evidences at the scale of the individual particles. Finally, we saw that from an experimental point of view, testing the uniformity of the measure over the blocked configurations is a chimera, until a full microscopic description of the system is provided. However, in the meantime looking for relevant extensive and intensive thermodynamical parameters is a key step for achieving a thermodynamical description of non-hamiltonian systems. In this matter we have stressed that one must be careful with potential long range correlations and associated non-extensivity.

Finally, let us suggest some further developments in the field. In the first part, we have seen how to define a thermodynamical equivalent of the temperature for stationary non-hamiltonian dynamics with a conserved quantity. Kurchan has proposed to extend the definition of the effective temperature obtained in the glassy regime for thermal glasses, to the case of a-thermal systems [48]. It would be of great interest to relate both approaches. One way for instance would be to study glassy regimes in a modified version of the model introduced by Bertin et al [10]. Given the strength of the similarities between granular media close to the jamming transition and the super-cooled liquids close to the glass transition, and given the rather easy access to the details of the particles dynamics in the case of the granular media, it would be of great benefit to further investigate the mechanisms underlying the development of the dynamical heterogeneities. Finally, given the possibility of extracting intensive parameters from the free volume distributions inside a granular packing, it is now a priority to test whether some of these parameters equilibrate between subsystems.

References

[1] R. Stinchcombe A. Lefèvre, L. Berthier. cond-mat/0410741, 2003.

[2] B. Abou and F. Gallet. Probing an nonequilibrium einstein relation in an aging colloidal glass. *Phys. Rev. Lett.*, 93(160603), 2004.

[3] H.C. Andersen. *PNAS*, 102:6686, 2005.

[4] A. Barrat, J. Kurchan, V. Loreto, and M. Sellitto. Edwards' measures for powders and glasses. *Phys. Rev. Lett.*, 85:5034–5037, 2000.

[5] A. Barrat, J. Kurchan, V. Loreto, and M. Sellitto. Edwards' measures: a thermodynamic construction for dense granular media and glasses. *Phys. Rev. E*, 63:51301, 2001.

[6] J. L. Barrat and W. Kob. *Europhys. Lett.*, 46:637, 1999.

[7] L. Bellon, S. Ciliberto, and C. Laroche. *Europhys. Lett.*, 53:511, 2001.

[8] L. Berthier. *Phys. Rev. E*, 69(020201(R)), 2004.

[9] L. Berthier and J. L. Barrat. *Phys. Rev. Lett.*, 89(095702), 2002.

[10] E. Bertin, O. Dauchot, and M. Droz. Temperature in nonequilibrium systems with conserved energy. *Phys. Rev. Lett.*, 93:230601, 2004.

[11] E. Bertin, O. Dauchot, and M. Droz. Non-equilibrium temperatures in steady-state systems with conserved energy. *Phys. Rev. E*, 71:046140, 2005.

[12] J.P. Bouchaud. Granular media: some ideas from statistical physics. lecture given in Les Houches, 2002.

[13] T. Boutreux and P. G. de Gennes. *Physica A*, 244:59, 1997.

[14] J. J. Brey, A. Prados, and B. Sanchez-Rey. Thermodynamic description in a simple model for granular compaction. *Physica A*, 275:310–324, 2000.

[15] J. Casas-Vasquez and D. Jou. *Rep. Prog. Phys.*, 66:1937, 2003.

[16] A. Crisanti and F. Ritort. *J. Phys A: Math. Gen.*, 36(R181), 2003.

[17] F. Da Cruz, F. Lechenault, O. Dauchot, and E. Bertin. Free volume distributions inside a bidimensional granular medium. In *Powders and Grains 2005, Stuttgart*, 2005.

[18] L. F. Cugliandolo and J. Kurchan. *Phys. Rev. Lett.*, 71:173, 1993.

[19] L. F. Cugliandolo, J. Kurchan, and L. Peliti. *Phys. Rev. E*, 55:3898, 1997.

[20] L.F. Cugliandolo and J.L. Iguain. *Phys. Rev. Lett.*, 85:3448, 2000.

[21] G. D'Anna and G. Gremaud. The jamming route to the glass state in a weakly perturbed granular media. *Nature*, 413:407–409, 2001.

[22] G. D'Anna, P. Mayor, A. Barrat, V. Loreto, and F. Nori. Observing brownian motion in vibration-fluidized granular matter. *Nature*, 424:909–911, 2003.

[23] O. Dauchot, G. Marty, and G. Biroli. Dynamical heterogeneity close to the jamming transition in a sheared granular material. condmat0507152 submitted to Phys. Rev. Lett., 2005.

[24] D.S. Dean and A. Lefèvre. Steady state behavior of mechanically perturbed spin glasses and ferromagnets. *Phys. Rev. E*, 64:046110, 2001.

[25] B. Diu, C. Guthmann, D. Lederer, and B. Roulet. Hermann, Paris, 1989.

[26] B. Doliwa and A. Heuer. *Phys. Rev. Lett.*, 80:4915, 1998.

[27] B. Doliwa and A. Heuer. *J. Phys. Cond. Mat.*, 11:A227, 1999.

[28] C. Donati, J. F. Douglas, W. Kob, S. J. Plimpton, P. H. Poole, and S. C. Glotzer. *Phys. Rev. Lett.*, 80:2338, 1998.

[29] C. Donati, S. Franz, S.C. Glotzer, and G. Parisi. *J. Non-Cryst. Sol.*, 307:215–224, 2002.

[30] M.A. Ediger. *Annu. Rev. Phys. Chem.*, 51:99, 2000.

[31] S. F. Edwards. The role of entropy in the specification of a powder. In A. Mehta, editor, *Granular Matter: An Interdisciplinary approach*, pages 121–140, New-York, 1994. Springer-Verlag.

[32] S.F. Edwards and D.V. Grinev. *Phys. Rev. Lett.*, 82(5397), 1999.

[33] S.F. Edwards and R.B.S. Oakeshott. Theory of powders. *Physica A*, 157:1080–1090, 1989.

[34] S. Franz and G. Parisi. *J. Phys. Cond. Matt.*, 12:6353, 2000.

[35] C. Godrèche and J.M. Lück. Metastability in zero-temperature dynamics: Statistics of attractors. *J. Phys. Cond. Matt.*, 2005. to appear, condmat/0412077.

[36] M. Goldstein. *J. Chem. Phys.*, 51:3728, 1969.

[37] T. S. Grigera and N. E. Israeloff. *Phys. Rev. Lett.*, 83:5038, 1999.

[38] G.Williams and D.C.Watts. *Trans. Faraday Soc.*, 66:80, 1970.

[39] D. Herisson and M. Ocio. *Phys. Rev. Lett.*, 88(257202), 2002.

[40] A. Heuer. *Phys. Rev. E*, 56:730, 1997.

[41] M.M. Hurley and P. Harrowell. *Phys. Rev. E*, 52:1694, 1995.

[42] C. Josserand, A. V. Tkachenko, D. M. Mueth, and H. M. Jaeger. Memory effect in granular materials. *Phys. Rev. Lett.*, 85:3632–3635, 2000.

[43] A. Kabla and G. Debregeas. Contact dynamics in a gentlyvibrated granular pile. *Phys. Rev. Lett.*, 92(035501), 2004.

[44] J. B. Knight, C. G. Fandrich, C. N. Lau, H. M. Jaeger, and S. R. Nagel. Density relaxation in a vibrated granular media. *Phys. Rev. E*, 51:3957–3963, 1995.

[45] W. Kob and H. C. Andersen. *Phys. Rev. E*, 51:4626–4641, 1995.

[46] W. Kob and H. C. Andersen. *Phys. Rev. E*, 52:4134–4153, 1995.

[47] R. Kohlrausch. *Pogg. Ann. Phys. Chem.*, 91:179, 1854.

[48] J. Kurchan. Emergence of macroscopic temperatures in systems that are not thermodynamical microscopically: towards a thermodynamical description of slow granular rheology. *J. Phys. Condens. Matter*, 29:6611–6617, 2000.

[49] J. Kurchan. In A.J. Liu and S.R. Nagel, editors, *Jamming and Rheology : Constrained dynamics on Microscopic and Macroscopics scales*, pages 72–79, London, 2001. Taylor and Francis.

[50] N. Lacevic, F.W. Starr, T.B. Schroeder, and S.C. Glotzer. *J. Chem. Phys*, 119:7372, 2003.

[51] L.D. Landau and E.M. Lifshitz. Pergamon, New-York, 1970.

[52] A. J. Liu and S. R. Nagel. Jamming is not just cool anymore. *Nature*, 396:21–22, 1998.

[53] H. A. Makse and J. Kurchan. Testing the thermodynamic approach to granular matter with a numerical model of a decisive experiment. *Nature*, 415:614–616, 2002.

[54] G. Marty and O. Dauchot. Subdiffusion and cage effect in a sheared granular material. *Phys. Rev. Lett.*, 94:015701, 2005.

[55] R. Monasson. The structural glass transition and the entropy of the metastable states. *Phys. Rev. Lett.*, 75(15):2847, 1995.

[56] M. Nicolas, P. Duru, and O. Pouliquen. Compaction of a granular material under cyclic shear. *Eur. Phys. J. E*, 3:309–314, 2000.

[57] E.R. Nowak, J.B. Knight, E. Ben-Naim, H.M. Jaeger, and S.R. Nagel. Density fluctuations in vibrated granular materials. *Phys. Rev. E*, 57(2):1971, 1998.

[58] G. Parisi. *Phys. Rev. Lett.*, 79:3660, 1997.

[59] P. Philippe and D. Bideau. Compaction dynamics of a granular medium under vertical tapping. *Europhys. Lett.*, 60:677–683, 2002.

[60] P. Philippe and D. Bideau. Granular medium undervertical tapping: Change of compaction and convection dynamics around the liftoff threshold. *Phys. Rev. Lett.*, 91:104302, 2003.

[61] O. Pouliquen, M. Belzons, and M. Nicolas. Fluctuating particle motion during shear induced granular compaction. *Phys. Rev. Lett.*, 91:014301, 2003.

[62] M. Schröter, D.I. Goldman, and H.L. Swinney. Stationnary state volume fluctuations in a granular medium. *Phys. Rev. E*, 71(030301(R)), 2005.

[63] F. Sciortino and P. Tartaglia. *Phys. Rev. Lett.*, 86:107, 2001.

[64] C. Song, P. Wang, and H. A. Makse. Experimental measurement of an effective temperature for jammed granular materials. *Proc. Nat. Acad. Sci.*, 102:2299–2304, 2005.

[65] F.H. Stillinger and T.A. Weber. *Phys. Rev. A*, 25:978, 1982.

[66] F.H. Stillinger and T.A. Weber. *Science*, 225:983, 1984.

[67] C. Toninelli, M. Wyart, G. Biroli, L. Berthier, and J.-P. Bouchaud. *Phys. Rev. E*, 71(041505), 2005.

[68] E. R. Weeks, J.C. Crocker, A.C. Levitt, A. Schofield, and D.A. Weitz. *Science*, 287:627, 2000.

[69] E. R. Weeks and D.A. Weitz. Properties of cage rearrangements observed near the colloidal glass transition. *Phys. Rev. Lett.*, 89:095704, 2002.

[70] S. Whitelam, L. Berthier, and J. P. Garrahan. *Phys. Rev. Lett.*, 92:185705, 2004.